Contamination of planktonic food webs in the Mediterranean Sea: Setting the frame for the MERITE-HIPPOCAMPE oceanographic cruise (spring 2019)

Marc Tedetti, Jacek Tronczynski, François Carlotti, Marc Pagano, Sana Ben Ismail, Cherif Sammari, Malika Bel Hassen, Karine Desboeufs, Charlotte Poindron, Amel Bellaaj Zouari, et al.

Contamination of planktonic food webs in the Mediterranean Sea: Setting the frame for the MERITE-HIPPOCAMPE oceanographic cruise (spring 2019)

Marc Tedetti[a*], Jacek Tronczynski[b], François Carlotti[a], Marc Pagano[a], Sana Ben Ismail[c], Cherif Sammari[c], Malika Bel Hassen[c], Karine Desboeufs[d], Charlotte Poindron[d], Sandrine Chifflet[a], Amel Bellaaj Zouari[c], Moufida Abdennadher[c], Sirine Amri[c], Daniela Bănaru[a], Lotfi Ben Abdallah[c], Nagib Bhairy[a], Ismail Boudriga[c], Aude Bourin[e], Christophe Brach-Papa[f], Nicolas Briant[b], Léa Cabrol[a], Cristele Chevalier[a], Lassaad Chouba[c], Sylvain Coudray[f], Mohamed Nejib Daly Yahia[g], Thibault de Garidel-Thoron[h], Aurélie Dufour[a], Jean-Claude Dutay[i], Boris Espinasse[j], Pamela Fierro-González[a], Michel Fornier[a], Nicole Garcia[a], Franck Giner[k], Catherine Guigue[a], Loïc Guilloux[a], Asma Hamza[c], Lars-Eric Heimbürger-Boavida[a], Stéphanie Jacquet[a], Joel Knoery[b], Rim Lajnef[c], Nouha Makhlouf Belkahia[l,m], Deny Malengros[a], Pauline L. Martinot[a], Anthony Bosse[a], Jean-Charles Mazur[h], Marouan Meddeb[m,n], Benjamin Misson[o], Olivier Pringault[a], Marianne Quéméneur[a], Olivier Radakovitch[h,k], Patrick Raimbault[a], Christophe Ravel[f], Vincent Rossi[a], Chaimaa Rwawi[a], Asma Sakka Hlaili[m,n], Javier Angel Tesán-Onrubia[o], Bastien Thomas[b], Melilotus Thyssen[a], Noureddine Zaaboub[c], Cédric Garnier[o]

[a] Aix Marseille Univ., Université de Toulon, CNRS, IRD, MIO, Marseille, France

[b] Ifremer, CCEM Contamination Chimique des Ecosystèmes Marins, F-44000 Nantes, France

[c] Institut National des Sciences et Technologies de la Mer (INSTM), 28, rue 2 mars 1934, Salammbô 2025, Tunisia

[d] Université Paris Cité et Université Paris-Est Creteil, CNRS, LISA, F-75013 Paris, France

[e] IMT Nord Europe, Institut Mines-Télécom, Univ. Lille, Centre for Energy and Environment, F-59000 Lille, France

[f] Ifremer, Unité Littoral, Laboratoire Environnement Ressources Provence Azur Corse, Zone portuaire de Brégaillon, CS 20330, 83507 La Seyne-sur-Mer Cedex, France

[g] Environmental Sciences Program, Department of Biological and Environmental Sciences, College of Arts and Sciences, Qatar University, PO Box 2713, Doha, Qatar

[h] Aix Marseille Univ., CNRS, IRD, Collège de France, INRAE, CEREGE, 13545 Aix-en-Provence Cedex 4, France

[i] Laboratoire des Sciences du Climat et de l'Environnement LSCE/IPSL, CEA-CNRS-UVSQ, Université Paris-Saclay, 91191 Gif-sur-Yvette, France

[j] Department of Arctic and Marine Biology, UiT The Arctic University of Norway, Tromsø, Norway

[k] Institut de Radioprotection et de Sûreté Nucléaire (IRSN), PSE-SRTE-LRTA, Cadarache, France

[l] Université de Carthage, Faculté des Sciences de Bizerte, Bizerte, Tunisia

[m] Université de Tunis El Manar, Faculté des Sciences de Tunis, Laboratoire des Sciences de l'Environnement, Biologie et Physiologie des Organismes Aquatiques LR18ES41, Tunis, Tunisia

[n] Université de Carthage, Faculté des Sciences de Bizerte, Laboratoire de Biologie Végétale et Phytoplanctonologie, Bizerte, Tunisia

[o] Université de Toulon, Aix Marseille Univ., CNRS, IRD, MIO, Toulon, France

* Correspondence: Marc Tedetti; marc.tedetti@mio.osupytheas.fr

For submission to Marine Pollution Bulletin – Special issue "*Plankton and Contaminants in the Mediterranean Sea: Biological pump and interactions from regional to global approaches*"

Revised version, 09 February 2023

Abstract

This paper looks at experiential feedback and the technical and scientific challenges tied to the MERITE-HIPPOCAMPE cruise that took place in the Mediterranean Sea in spring 2019. This cruise proposes an innovative approach to investigate the accumulation and transfer of inorganic and organic contaminants within the planktonic food webs. We present detailed information on how the cruise worked, including 1) the cruise track and sampling stations, 2) the overall strategy, based mainly on the collection of plankton, suspended particles and water at the deep chlorophyll maximum, and the separation of these particles and planktonic organisms into various size fractions, as well as the collection of atmospheric deposition, 3) the operations performed and material used at each station, and 4) the sequence of operations and main parameters analysed. The paper also provides the main environmental conditions that were prevailing during the campaign. Lastly, we present the types of articles produced based on work completed by the cruise that are part of this special issue.

Key words: contaminants, plankton, Mediterranean Sea, size fractions, bioaccumulation, atmospheric deposition

1. Introduction

Plankton is recognised as a key gateway of inorganic and organic contaminants into the marine food web (Berroralbiz et al., 2011; Tao et al., 2018; Chouvelon et al., 2019; Li et al., 2021). Phytoplankton exposure to contaminants is mainly *via* water. Phytoplankton cells have a high surface area-to-volume ratio and thus large areas for exchanges, and consequently display high capacities for adsorbing and absorbing and thus bioconcentrating dissolved contaminants (Martin and Knauer, 1973; Fan and Reinfelder, 2003; Heimbürger et al., 2010; Lee and Fisher, 2016; Chouvelon et al., 2019). Contaminant bioconcentration in phytoplankton, thought to be governed mainly by partition equilibrium processes between the cells and the surrounding water (Frouin et al., 2013) even though cell growth conditions may prevent contaminants from reaching thermodynamic equilibrium (Swackhamer and Skoglund, 1993), tends to increase with decreasing size of algal cells (Fan and Reinfelder, 2003).

Bioaccumulation processes in zooplankton are highly complex due to 1) entry of contaminants by both the water aqueous phase (bioconcentration) and diet, 2) trophic interactions and/or transfers between phytoplankton and herbivorous, carnivorous and omnivorous zooplankton, and 3) the contaminant elimination processes used by these organisms, including metabolization, excretion and passive release (Tiano et al., 2014; Alekseenko et al., 2018; Tao et al., 2018; Thomas et al., 2018; Li et al., 2020). The fact that all these processes can act simultaneously in the same or opposite directions makes it difficult to understand the variability of contaminant concentrations within the planktonic food web, which may ultimately display biomagnification (increasing contaminant concentrations with trophic level), bioreduction (decreasing contaminant concentrations with trophic level) or no clear pattern (Nizzetto et al., 2012; Tiano et al., 2014; Strady et al., 2015; Tao et al., 2017a, b;

100 Alekseenko et al., 2018; Chouvelon et al., 2019; Tang et al., 2020; Castro-Jiménez et al.,
101 2021; Li et al., 2021).

102 One important biogeochemical implication of contaminant uptake by plankton is the
103 role as a "biological pump" for contaminant sequestration (Dachs et al., 2002; Galbán-
104 Malagón et al., 2012; Duran and Cravo-Laureau, 2016; González-Gaya et al., 2019; Tang et
105 al., 2020). Contaminants bioconcentrated/bioaccumulated within planktonic organisms
106 subsequently get transferred to higher trophic levels or to deep waters and sediment through
107 sinking particles. During phytoplankton blooms, contaminant uptake by plankton depletes the
108 contaminant loads in the dissolved phase of the water column and increases contaminant air-
109 water fluxes, sinking particle fluxes and sequestration in sediments (Berrojalbiz et al., 2011;
110 Nizzetto et al., 2012; Everaert et al., 2015; Morales et al., 2015; Casal et al., 2017; Ding et al.,
111 2021).

112 The phosphorus-limited Mediterranean Sea is globally classified as an oligotrophic
113 marine area (D'Ortenzio and d'Alcalà, 2009; The Mermex Group, 2011; Marañón et al.,
114 2021) dominated by small phytoplankton (i.e., pico- and nano-sized fractions) (Uitz et al.,
115 2006; Hunt et al., 2017; Mayot et al., 2017; Leblanc et al., 2018; Salhi et al., 2018; Ramirez-
116 Romero et al., 2020), even though the occurrence of regional phytoplankton blooms (bloom
117 bioregions, ecoregions; D'Ortenzio and Ribera d'Alcalà, 2009; Berline et al., 2014;
118 Reygondeau et al., 2017; Ayata et al., 2018) leads to periods of coexistence of numerous
119 microalgal groups (Siokou-Frangou et al., 2010; El Hourany et al., 2019).

120 Another feature of the Mediterranean Sea is its high exposure to chemical
121 contamination (Hinrichsen, 1990; The Mermex Group, 2011; UNEP, 2012). Indeed, the
122 intense human activities in its 23 bordering countries induce significant inputs of various
123 chemical contaminants, while its semi-closed geography limits possibilities for diluting them.
124 Contaminants are brought to the Mediterranean mainly by major and smaller river systems

(Elbaz-Poulichet et al., 2001; Radakovitch et al., 2008; Sicre et al., 2008; Guigue et al., 2014; Köck-Schulmeyer et al., 2021) but also *via* effluents, runoffs, groundwater, and maritime activities (Tedetti et al., 2010; Oursel et al., 2013; Tornero and Hanke, 2016; Fourati et al., 2018; Jacquet et al., 2021; Llamas-Dios et al., 2021) as well as atmospheric deposition (Lipiatou and Albaigés, 1994; Heimbürger et al., 2011; Castro-Jiménez et al., 2017; Barhoumi et al., 2018; Desboeufs et al., 2022). Studies have demonstrated that atmospheric deposition is the major source of contaminants in remote/open sea areas (Dachs and Méjanelle, 2010; González-Gaya et al., 2019; Jiskra et al., 2021; Cossa et al., 2022).

An interesting feature of the bioaccumulation of contaminants in the Mediterranean Sea is that the recorded contamination levels are significantly higher in its predatory species (crustaceans, sharks, teleost fish) than in congeneric species of the Atlantic Ocean (Cossa and Coquery, 2005; Bodiguel et al., 2009; Chouvelon et al., 2018). This difference may be related (but not solely) to the enhanced ability of the Mediterranean planktonic food webs to bioaccumulate certain contaminants, such as mercury (Hg) (Cossa and Coquery, 2005; Harmelin-Vivien et al., 2009; Chouvelon et al., 2018, 2019; Cossa et al., 2022), which further underscores the potential key role of the planktonic compartment in the transfer and accumulation of contaminants in the Mediterranean Sea. Furthermore, contaminant-plankton interactions in the Mediterranean Sea are expected to evolve in the coming years, as it has been identified as a hotspot for climate change due to its high reactivity to external forcing, particularly variations in water, energy and matter fluxes that will affect its circulation, biogeochemical fluxes and ecosystem functioning (Lejeusne et al., 2010; The Mermex Group, 2011; Ser-Giacomi et al., 2020).

However, there are still key gaps in our understanding around the actual ability of plankton to accumulate and transfer contaminants (i.e., the role of plankton as a biological pump of contaminants), especially its small size fractions, i.e., pico- and nano-plankton. This

lack of knowledge partly comes from methodological difficulties in: 1) collecting and separating plankton into its various size fractions from pico- to macro-plankton, separating bacterio-, phyto- from zoo-plankton, and separating non-living suspended particulate matter from plankton, 2) obtaining sufficient material in each of these fractions to perform trace-level chemical analyses, and 3) clearly identifying the trophic relationships between planktonic size fractions in the presence of detritus (particularly in smaller size fractions) and mixing of different trophic levels within each size fraction.

In this context, the MERITE-HIPPOCAMPE cruise aimed to evaluate the accumulation and transfer of a hugely diverse range of inorganic and organic contaminants at the atmosphere-water-plankton interfaces and within the planktonic food webs, i.e., phyto-, zoo- and bacterio-plankton, along a North-South transect in the Mediterranean Sea. This ultimately to quantify the role of Mediterranean plankton as a biological pump of contaminants, focusing on contaminant transfers into the planktonic food webs. The main collection area for plankton, suspended particles and water is the deep chlorophyll maximum (DCM), which may be considered as the layer with the highest biomasses of plankton, mainly phytoplankton, but also zooplankton. The plankton size fractions investigated include pico- (0.2–2 µm), nano- (2–20 µm), micro- (20–200 µm) and meso-plankton (200–2000 µm). The contaminants examined are trace metals, organometals and metalloids (As, Cd, Cr, Cu, Fe, Hg, MeHg, Mn, Ni, Pb, Sb, Zn…), organic contaminants (PAHs, PCBs, PBDEs, PFASs), radionuclides (^{137}Cs), and microplastics. The specific objectives of the cruise are: 1) to determine the contaminant concentration levels in various planktonic compartments (phyto-, zoo- and bacterio-plankton), suspended particles and water (dissolved phase), as well as atmosphere and, 2) to assess the role of dry/wet atmospheric deposition as a source of contaminants for marine waters, especially in offshore areas, 3) to gauge how contaminant accumulations and transfers are influenced by plankton in terms of size and community structures, trophic

interactions and biochemical content, and 4) to establish the link between habitat characteristics and concentration levels of contaminants in plankton. The questions addressed by the MERITE-HIPPOCAMPE cruise are summarised in Fig. 1. In this paper, we first present the implementation of the cruise project in terms of strategy, study stations, material used, operations performed, sequence of operations, and main parameters analysed. We then work up from a joint dataset to provide the main meteorological, hydrological, and biogeochemical conditions prevailing during the cruise. Lastly, we introduce the types of articles produced through the MERITE-HIPPOCAMPE cruise that are part of this special issue.

2. Implementation of the cruise

2.1. Research strategy

The overall research strategy for our oceanographic cruise was as follows:

1) Investigate areas of contrasted ecological characteristics in the north and south of the Mediterranean Sea. The selected period was the spring bloom, crossing primary production and bloom areas as defined by D'Ortenzio and d'Alcalà (2009) as well as various fishing zones, urbanised bays, and consensus regions as defined by Ayata et al. (2018) (Fig. 2a, b; Fig. S1).

2) Characterise the water column in these sampling sites in terms of physical and biogeochemical properties through *in situ* physical and optical measurements, and determine the DCM.

3) Implement ultra-clean on-board conditions for the collection and treatment of water and plankton samples for ultra-trace-level analyses of inorganic and organic contaminants.

4) Collect large amounts of plankton, suspended particles, and water (dissolved phase) in the DCM and, in a lesser extent, surface/subsurface waters (0–5 m depth) (Fig. 3). The choice of focusing our sampling on the DCM was motivated by the need to 1) collect a high biomass of plankton from the same location to determine the concentration levels of a wide range of contaminants, and over a broad spectrum of planktonic size fractions, and 2) be located in a relevant area for pelagic trophic interactions in both the coastal and marine areas.

5) Separate these large amounts of plankton and particles into various size fractions (from 0.2 µm to > 2000 µm) by filtration or sieving (Fig. 3).

6) Share the size fractioned samples for analysis of a battery of parameters, including (i) contaminants, with trace metals, organometals and metalloids (As, Cd, Cr, Cu, Fe, Hg, MeHg, Mn, Ni, Pb, Sb, Zn, etc.), organic contaminants (PAHs, PCBs, PBDEs, PFASs), radionuclides (^{137}Cs) and microplastics, (ii) biomass, size structure, taxonomy, cytometry, diversity and pigment composition of plankton, and (iii) biogeochemical parameters, with nutrients, total chlorophyll *a* (TChl*a*), suspended particulate matter (SPM), dissolved and particulate organic matter, C and N isotopic ratios (δ^{13}C, δ^{15}N), and biochemical compounds (carbohydrates, proteins, lipids) (Fig. 3).

7) Combine several methods (taxonomy, optical measurements, chemical analyses) to tentatively distinguish the contributions of living (plankton) and non-living (detrital) materials to contaminant accumulation and transfers.

8) Collect on-board samples of atmospheric wet deposition (rain) to assess their potential importance as a source of contaminants for marine water and plankton. The collection of atmospheric samples was also done in parallel on the coast by setting up two ground stations, located in the northern part (Marseille, France) and southern part (Sfax, Tunisia) of the Mediterranean basin (Fig. 2a), in which atmospheric total (dry and wet)

deposition were measured on a regular (bi-monthly or monthly) basis from March 2019 to June 2020, i.e., before, during, and after the oceanographic cruise.

9) Sample small pelagic plankton-feeding fishes in Tunisian waters (see sampling positions in Fig. 2a). The fish samples were analysed for a number of contaminants in order to set bioaccumulation factors for higher trophic levels.

2.2. Cruise track and study stations

The MERITE-HIPPOCAMPE cruise took place in spring 2019, from April 13 to May 14, on board the French Research Vessel (R/V) *Antea* along a North-South transect (round trip) in the Mediterranean Sea, from the French coast (La Seyne-sur-Mer, Northwestern Mediterranean) to the Gulf of Gabès in Tunisia (Southeastern Mediterranean) (Tedetti and Tronczynski, 2019) (Fig. 2a, b). Leg 1 (13–28 April 2019) ran the southward transect, between La Seyne-sur-Mer and Tunis, with sampling at five stations: St2, St4, St3, S10, and St11 (in this chronological order). Leg 2 (30 April–14 May 2019) covered first the end of the southward transect (from Tunis to the Gulf of Gabès), and then the return trip back northward from the Gulf of Gabès to La Seyne-sur-Mer. Five stations were sampled during leg 2: St15, St17, St19, St9 and St1 (in this chronological order). Five stations (St1–St4, St9) were situated in the French area, two stations (St10, St11) in the Italian area, and three stations (St15, St17, St19) in the Tunisian area (Fig. 2a, b; Table 1).

The ten stations were chosen according to different criteria based on physical, biogeochemical and biological conditions and anthropogenic pressures (Fig. 2a; Fig. S1; Table 1). St1 and St4 were located in the urbanised bays opposite the cities of Toulon and Marseille, respectively, and thus submitted to strong anthropogenic pressures. St4 was the SOLEMIO station, which is part of the French national coastal observation monitoring network SOMLIT (http://somlit.epoc.u-bordeaux1.fr/fr/). St1 and St4 were “intermittent

bloom" areas or "bloom" areas according to D'Ortenzio and d'Alcalà (2009) based on SeaWiFS satellite observations of surface TChl*a* concentration. St2 and St3 were situated offshore of Toulon and Marseille, respectively. St2 was at the limit of the continental shelf and the boundary of the Ligurian consensus region (Ayata et al., 2018) (Fig. S1). St3, situated at the southeast entrance to the Gulf of Lion's continental shelf, was the JULIO station, which is dedicated to the study of intrusions of the Ligurian-Provençal current (Barrier et al., 2016). St2 and St3 were considered "intermittently bloom" areas or "bloom" areas (D'Ortenzio and d'Alcalà, 2009). These stations (St1–St4) have hosted in the past or continue to host visits serving several monitoring networks such as SOMLIT and ROMARIN, and projects including MERMEX-MERITE, COSTAS and IBISCUS.

St9 corresponds to offshore station 1 of the PEACETIME cruise (Guieu et al., 2020). It was located north of the North Balearic thermal Front (NBF), at the boundary of the Ligurian consensus region (Ayata et al., 2018), in the winter convection area (Fig. S1). The NBF, which is one of the main consensus frontiers of the Mediterranean Sea (Ayata et al., 2018), is found between the Balearic Islands and Sardinia, but its position spans a large area and can vary with wind conditions and seasons (Barral et al., 2021). St10 (offshore station 2 of the PEACETIME cruise) was situated south of St9, very close to the NBF. Although St10 was positioned south of the average position of the NBF, it was in fact located slightly north of the front which had moved further south during the sampling period (Rwawi et al., in prep.). St11 (offshore station 3 of the PEACETIME cruise) was plainly positioned south of the NBF, in the Algerian consensus region (Ayata et al., 2018) (Fig. S1). St10 and St11 were characterised by the presence of intense mesoscale eddies: St10 was rather situated between one anticyclonic and one cyclonic eddy, while St11 was located within an anticyclonic eddy (Rwawi et al., in prep.). St9, St10, and St11 are referred to as "bloom", "intermittent bloom"

and “no bloom” areas, respectively, according to the D’Ortenzio and d’Alcalà (2009) system (Fig. 2a; Table 1).

St15, situated in the Gulf of Hammamet (Tunisia), was close to the Sicily Channel, which plays host to the exchanges between the two (Western and Eastern) Mediterranean basins, and submitted to the possible entrance of the Atlantic Tunisian Current branch, also called the Atlantic-Ionian stream. St17 (north of the Gulf of Gabès) and St19 (south of the Gulf of Gabès) were located at the boundary of and within the Gabès consensus region, respectively (Ayata et al., 2018) (Fig. S1), and are typified by shallow waters, strong influences of tidal pull (the highest of the Mediterranean; amplitude > 2 m) and the Atlantic Tunisian Current. St17 and St19 are also characterised by nutrient inputs from Saharan dust deposition or sediment resuspension and the resulting high planktonic productivity levels (Béjaoui et al., 2019). Moreover, given its cumulative index of warming, overfishing and pollution effects, the Gulf of Gabès has recently been recognised as a hotspot of anthropogenic pressures within the Mediterranean Sea (Reygondeau et al., 2014). St15, St17 and St19 were zones marked by a high density of small pelagic fish and considered as “no bloom” (St15) or “coastal bloom” areas (St17, St19) based on the D’Ortenzio and d’Alcalà (2009) system. These stations (St15-St19) have been investigated in the past in the framework of the Tunisian POEMM and ESSATEL programs (Fig. 2a; Fig. S1; Table 1).

Due to rough sea conditions that occurred during sampling of St19 (south of the Gulf of Gabès; Fig. 2a, b), the ship went to shelter, first off the island of Djerba and then off the city of Zarzis (Fig. 2a, b), before returning to station St19 to finish work between May 3 and 4. During the transit between off Djerba and off Zarzis, atmospheric deposition sampling was carried out following an intense episode of Saharan dust deposition.

Besides the ten stations prospected from the R/V *Antea*, two other stations (T2 and T4) were sampled in the Tunisian waters during leg 2 (2–3 May 2019) on board the R/V *Hannibal*

298 for trawling small pelagic fishes. T2 was located in the Gulf of Gabès not far from St19,
299 whereas T4 was situated in the Gulf of Tunis. The duration of trawling was 40 min at T2 and
300 90 min at T4 (Fig. 2a; Table 2). The fish species captured by trawling were anchovy, sardine,
301 sardinella, and mackerel (Lajnef et al., in prep.).
302
303 ### 2.3. Equipment and operations
304 At each of the ten stations, the following sampling equipment was deployed and the
305 following operations were performed at sea and on board the R/V *Antea*.
306 *2.3.1. Water sampling with Niskin and Go-Flo bottles and subsequent in-line*
307 *filtration.* A trace metal-clean carousel equipped with ten 12-L bottles (1 Niskin, 5 Niskin X,
308 4 Go-Flo) and a conductivity-temperature-depth probe (CTD; Seabird SBE 911*plus*),
309 mounted with photosynthetically available radiation (PAR) (Biospherical), TChl*a*
310 fluorescence (Aqua Tracka, Chelsea ctg), dissolved oxygen (O_2) (SBE 43), dissolved organic
311 matter (DOM) fluorescence (WETStar, WETLabs) and transmittance (C-Star, WETLabs)
312 sensors, was deployed from the ship's moon pool *via* the electro-mechanical (conducting)
313 cable (Table S1; Fig. S2a). Vertical profiles were collected over the depth range 0–250 m or
314 surface-to-bottom when depth was < 250 m, and seawater was sampled at two depths: 5 m or
315 the DCM identified based on TChl*a* profiles. Seven bottles (4 Niskin X and 3 Go-Flo) were
316 dedicated to DCM sampling, while three bottles (1 Niskin, 1 Niskin X and 1 Go-Flo) were
317 used for 5-m-depth sampling. The Go-Flo bottles were lowered into the water in open
318 position. At St9 and St10, sampling was also conducted down to 500-m depth to collect
319 seawater in the oxygen minimum zone (OMZ) identified based on O_2 profiles. At St9, water
320 was collected at 5 m, DCM and 440 m (identified as OMZ), whereas at St10 sampling was
321 carried out at 5 m, DCM, 100, 200, 300, 400 m (identified as OMZ) and 500 m. The Niskin X
322 bottles used here (model 101012X) are Niskin with a completely free Teflon-coated sample

chamber, Teflon-coated and externally-located stainless steel end plug closure springs, as well as Teflon-coated air valves and drainage taps. Before the cruise, all ten bottles were thoroughly washed with hydrochloric acid (HCl) 1 M, demineralized water and ultra-pure water (i.e., Milli-Q water from Millipore system, final resistivity of 18.2 MΩ cm). Before sampling, they were rinsed with seawater collected at 50-m and 170-m depth at the first station (St2). Between two casts, working on the deck of the ship, we covered the drainage taps and the top (upper stoppers) of the bottles with plastic bags to avoid any sample contaminations.

Once on board, after water collection at 5-m depth and in the DCM, the carousel with all the bottles was placed in the wet laboratory for in-line filtration (Table S1; Fig. S2b). For that purpose, the bottles were pressurised to 0.5 bar with argon (UN1006, compressed, 2.2) piped in using a silicon tubing system and quick-connect gas fittings replacing bottle air valves. The upper and lower stoppers of the Niskin bottles were held tight by home-made pairs of high-density polyethylene (HDPE) rods and clamps screwed at the top and bottom. A 10-cm-long piece of acid-cleaned silicon tubing was inserted into the drainage tap of each bottle, and a perfluoroalkoxy (PFA) filter holder (Savillex®, 25 or 47-mm diameter) was connected to the tubing. A graduated container collecting the filtered water served to indicate the exact volume filtered on each filter.

In-line filtration makes it possible to effectively filter large quantities of water in clean conditions and to recover the filters and filtered water samples for a battery of analyses. Filtration was done on pre-combusted (450 °C, 6 h), pre-weighed glass fibre filters (GF/F, Whatman) of 25 or 47-mm diameter (pore size: ~ 0.7 µm) for analyses of TChl*a*, pigments, SPM, particulate organic carbon (POC), particulate organic nitrogen (PON), stable isotopes of carbon and nitrogen ($\delta^{13}C$, $\delta^{15}N$), biochemical compounds (carbohydrates, lipids, proteins) and Hg on the size fraction > 0.7 µm. SPM measurements were done on (pre-weighed) 25-

mm and 47-mm-diameter GF/F filters rinsed with ultra-pure water after filtration in order to remove salts, but also on (pre-weighed) 47-mm-diameter GF/F filters that had not been rinsed with ultra-pure water (for which the amount of salts was estimated). Filtration was also done on pre-cleaned 0.2-µm-pore-size 47-mm-diameter mixed cellulose esters (MCE) filters for the analyses of trace metals/metalloids and microbial diversity on the size fraction > 0.2 µm, and on 0.8-µm-pore-size 47-mm-diameter pre-cleaned MCE filters for the analyses of copper (Cu) and zinc (Zn) isotopes on the size fraction > 0.8 µm. GF/F-filtered seawater (< 0.7 µm) was used for the analyses of nutrients, i.e., silicates [$Si(OH)_4$], nitrates (NO_3^-), nitrites (NO_2^-), phosphates (PO_4^{3-}) and ammonium (NH_4^+), dissolved organic carbon (DOC), and absorption of chromophoric DOM (a_{CDOM}), whereas 0.2-µm-filtered seawater was used for the analyses of dissolved trace metals/metalloids and Hg (Fig. 3; Table S1). Volume of seawater filtered ranged from 600 mL (25-mm GF/F filter for TChl*a*) to 12 L (47-mm GF/F filter for POC, PON, $\delta^{13}C$, $\delta^{15}N$, and biochemical compounds).

Raw (unfiltered) seawater was taken for the analyses of total trace metals/metalloids and Hg/MeHg, while seawater pre-filtered onto 100-µm silk was collected for phytoplankton taxonomy and cytometry analyses. Raw seawater from the DCM was also used to perform on-board experiments on microbial methylation/demethylation of Hg (at selected stations), while raw seawater collected at 5-m depth and in the DCM at St1, St9, S15 and St19 was used to conduct dilution experiments (see section 2.3.8). Most of these filtrations were also conducted on OMZ water (at St9 and St10) for the same analyses. Raw and 0.2-µm-filtered seawater at the different depths was also used for shipboard analyses of Hg (see section 2.3.9) (Table S1). Filter blanks were regularly run during the cruise: filters were treated as sample filters, either without passing any water on them or by rinsing with ultra-pure water, depending on the parameter. Detailed information on the in-line filtration from Go-Flo and Niskin bottles, including storage of samples, can be found in Fig. S3.

373 *2.3.2. In situ optical measurements.* A small CTD unit (SBE 19*plus*) equipped with
374 a TChl*a* fluorescence sensor (WETStar, WETLabs) was deployed from the moon pool on the
375 hydrographic cable, over the same depth range as the carousel (0–250 m or 0–bottom), to
376 timely determine the depth of the DCM between different sampling operations, in particular
377 just before McLane *in situ* pumps (see section 2.3.3) and MultiNet deployments (see section
378 2.3.5) (Table S1).
379 A laser optical plankton counter (LOPC, Rolls Royce) and laser *in situ* scattering
380 transmissometry-Holography (LISST-HOLO, Sequoia Scientific) were used together, fixed
381 on a small carousel, to provide information on the abundances and size spectra of particles
382 and plankton (> 20 µm for LISST-HOLO, > 100 µm for LOPC). Both systems were deployed
383 from the moon pool on the hydrographic cable. Vertical profiles were performed over the
384 depth range 0–250 m or 0–bottom (Table S1; Fig. S2c).
385 *2.3.3. In situ filtration with McLane pumps.* Four McLane Large Volume Water
386 Transfer System Samplers (WTS6-142LV, 4–8 L min^{-1}), hereinafter referred to as McLane *in*
387 *situ* pumps, were used to collect large amounts of particles and plankton over different size
388 fractions in the DCM. The four pumps were attached together with clamps and chains, and
389 deployed at the same time from the moon pool on the hydrographic cable to reach the DCM
390 (Fig. S2d). Pumping lasted between 40 and 60 min, giving an average ~ 240 L of water
391 filtered by each pump. Three successive casts of the four-pump system were carried out,
392 giving a total of 12 pumping runs done at each station (Table S1).
393 Three pumps (A, B, C) were each mounted with a regular 142-mm filter-holder
394 ("McLane holder") holding one 142-mm-diameter filter: one ~ 0.7-µm-pore-size pre-
395 combusted pre-weighed GF/F filter, one 0.8-µm-pore-size pre-cleaned MCE filter, or one 20-
396 µm-pore-size pre-cleaned Nylon filter. After installing the filters, the three McLane holders
397 were covered with a 60-µm-pore-size sock-type pre-filter so that the filtered particles size

fractions were 0.7–60, 0.8–60 and 20–60 µm. At three casts each, pumps A, B and C were able to sample nine filters for analysis of TChl*a*, SPM, POC, PON, $\delta^{13}C$, $\delta^{15}N$, biochemical compounds, PAHs, PCBs, PBDEs and Hg/MeHg on the GF/F filters (0.7–60-µm size fraction), analysis of trace metals/metalloids, Cu and Zn isotopes and microbial diversity on the MCE filters (0.8–60-µm size fraction), and analysis of microplastics on the Nylon filters (20–60-µm size fraction) (Fig. 3; Table S1; Fig. S4).

The fourth pump (D) was mounted with a mini-Multiple Unit Large Volume in-situ Filtration System (MULVFS) filter holder composed of baffle tubes on the top followed by successive baffle and filter support plates, for sequential filtration with three different filters (142-mm diameter) (Bishop and Wood 2008; Bishop et al., 2012). The baffles were designed to straighten the flow, suppress turbulence, and distribute particles evenly across the filter. The filter series used were either 1) one ~ 0.7-µm-pore-size pre-combusted, pre-weighed GF/F filter, one 2.7-µm-pore-size pre-combusted, pre-weighed GF/D filter, and one 20-µm-pore-size pre-cleaned Nylon filter, or 2) one 0.8-µm-pore-size pre-cleaned MCE filter, one 3-µm-pore-size pre-cleaned MCE filter, and one 20-µm-pore-size pre-cleaned Nylon filter. With its three casts, pump D was able to collect nine filters for the analysis of TChl*a*, SPM, POC, PON, $\delta^{13}C$, $\delta^{15}N$, biochemical compounds, and Hg/MeHg on the 0.7–2.7, 2.7–20, and > 20-µm size fractions, and trace metals/metalloids on the 0.8–3, 3–20, and > 20-µm size fractions (Fig. 3; Table S1; Fig. S4).

SPM measurements were made on (pre-weighed) 142-mm GF/F, GF/D and Nylon filters rinsed with ultra-pure water after filtration in order to remove residues of the seawater salts, but also on (pre-weighed) 142-mm GF/F filters not rinsed with ultra-pure water (for which the amount of salts was estimated). All filters were placed in glass boxes, plastic boxes or aluminium foil, depending on the parameter, and stored on board at –20 °C (Fig. S2e, f; Fig. S4). A special support was purpose-designed to accommodate/fix the filter holders in the

wet laboratory to facilitate the process of preparing the filters before deployment, and then handling, rinsing with ultra-pure water or direct drying (by connecting the filter holder to a vacuum pump) the filters after deployment (Fig. S2e, f). Before pump deployment, all the filter holder and filter systems were rinsed with ultra-pure water. Filter blanks were done at regular intervals during the cruise.

2.3.4. Water sampling and subsequent in-line filtration with an ASTI pump. Seawater was also sampled at ~ 10–20-m depth with a pneumatically-operated Teflon ASTI pump (model PFD2) set up on board and connected to Teflon tubing, which was weighted down and immersed from port side with the hydrology gallows (Table S1). The pumped seawater was filtered in-line onto a pre-combusted 142-mm GF/F filter using a 142-mm Teflon filtration holder. This filtration took place in the clean lab container (IFREMER, CNXU 300022/1) installed on the rear deck of the ship. Part of the filtered seawater was stored in three 20-L stainless steel jerrycans, while the other part was stored in a metal-free 50-L plastic container. This filtered seawater was used for sieving the large quantities of plankton collected with the Multiple Plankton Sampler. The filtered seawater stored in two of the stainless steel jerrycans was used exclusively for sieving on a stainless steel sieve column to obtain plankton samples for organic parameter analyses, and the filtered seawater stored in the plastic container was used exclusively for sieving on a nylon sieve column for analyses of inorganic parameters (see section 2.3.5). Filtered seawater from the third jerrycan was amended with 50 mL of dichloromethane, then shaken and degassed and stored in the container at ambient temperature for subsequent analyses of dissolved (< 0.7 µm) hydrocarbons (Guigue et al., in prep.) (Fig. 3; Table S1). All seawater containers (stainless steel and plastic) were rinsed several times with filtered seawater before sample collection.

2.3.5. Plankton sampling with a MultiNet and subsequent sieving. A Multiple Plankton Sampler (Midi type, Hydro-Bios), referred to hereafter as “MultiNet”, was

448 employed to collect plankton in the DCM. The MultiNet was composed of 5 individual
449 (exchangeable) 2.5-m-long nets with 0.25-m^2 apertures, a 60-µm mesh size, and cod ends of
450 the same mesh size, together with two Hydro-Bios flowmeters (one into the mouth and the
451 other on the side) to assess the volume of water filtered by the nets, plus a CTD sensor and a
452 TChl*a* fluorometer (Chelsea ctg). The MultiNet was connected *via* the electro-mechanical
453 cable to the operating computer to enable online monitoring of sensor feedback and opening
454 and closing of the nets, mainly based on flowmeter data and the amount of water passing
455 through the open net. It was operated from the stern A-frame. Since the device was deployed
456 horizontally in the DCM, the usual configuration (for vertical casts) was modified with a V-
457 fin deflector attached below the MultiNet and the five cod ends attached using a helicoidal
458 bucket connector (Fig. S2g, h). Ship speed while towing the MultiNet was ~ 2 knots (Table
459 S1). Once the five nets were filled (after 30 to 100 min depending on the station), the
460 MultiNet was hauled back on board, the cod ends were rinsed out with local seawater, and
461 their content was transferred to pre-cleaned 10-L HDPE bottles. The instrument was then
462 returned to the water. This operation ("cast") had to be repeated several times (between two
463 and eight horizontal casts, depending on the station) until we got sufficient amounts of
464 plankton. At St19, due to technical issues, the MultiNet was replaced by a square net with a 1-
465 m^2 aperture mounted with single 60-µm mesh-size net. Total filtered water volume with the
466 MultiNet/square net ranged from 314 (St2) to 2373 m^3 (St10).
467 In the clean on-board container lab, plankton collected in HDPE bottles was then size-
468 fractionated on 1) a column of five stainless steel sieves (60, 200, 500, 1000 and 2000-µm
469 mesh-size) by wet-sieving with the GF/F filtered seawater stored in stainless steel jerrycans
470 for subsequent analyses of organic parameters, and 2) a column of five nylon sieves (60, 200,
471 500, 1000 and 2000-µm mesh-size) by wet-sieving with the GF/F filtered seawater stored in
472 the plastic container for the subsequent analyses of inorganic parameters (Fig. S2i, j). The

filtered seawater was routed with a gentle flow to the top of the sieve column by the ASTI pump using Teflon tubing. The plankton size fractions recovered on the stainless-steel sieves were shared out and transferred to pre-combusted glass flasks for the analyses of POC, PON, $\delta^{13}C/\delta^{15}N$, biochemical compounds, PAHs, PCBs, PBDEs and PFASs, or to plastic flasks for zooplankton taxonomy and imagery, TChl*a* (60–200-µm size fraction only) and microbial diversity (60–200 and 200–500-µm size fractions only). The plankton size fractions recovered on the nylon sieves were shared out and transferred to pre-cleaned polypropylene flasks for the analyses of trace metals/metalloids, Hg and ^{137}Cs (Fig. 3; Table S1; Fig. S5). Planktonic biomass (in mg m^{-3} dry weight) was also determined in each of the size fractions (Fierro-González et al., 2023). All samples were stored at –20 °C except those for zooplankton taxonomy that were stored at ambient temperature after adding buffered formalin (Fig. S5).

2.3.6. Plankton and micro-plastic sampling with Triple and Manta nets. A triple net, equipped with 60, 120 and 200-µm mesh-sized nets each with 0.60-m aperture diameter was used to undertake two vertical tows over the depth 0–200 m (or 0–bottom if depth < 200 m), i.e., one tow for biomass, and one tow for taxonomy and imagery. The device was deployed from port side using hydrology gallows (Table S1; Fig. S2k). After collection, the cod-end contents from each of the three nets (first tow) were passed through GF/F filters that were stored in Petri dishes at –20 °C for biomass measurements, while the cod-end contents from the second tow were passed through a 60-µm sieve for volume reduction and transferred to 250-mL plastic tubes amended with 12.5-mL buffered formalin for taxonomy and imagery analyses. At St1, St9, S15 and St19, the contents of the 200-µm net were also collected to analyse chlorophyll gut-contents of mesozooplankton (see section 2.3.8).

Two Manta nets were used for horizontal tows in surface waters: one a 330-µm mesh size (1 tow, 3 knots, 20 min max) for microplastic analyses, and the other a 60-µm mesh size (1 tow, 1 knot, 10 min max) for microplastics and plankton (neuston) analyses, both deployed

from port side using hydrology gallows (Table S1). After collection, the content of the 330-µm Manta net was sieved successively through 5000 and 300-µm mesh-size sieves (if large items were present in the collectors) and transferred to a 1-L glass bottle added with formalin (4% final concentration). The content of the 60-µm Manta net was transferred to a 1-L glass bottle added with 50-mL buffered formalin.

2.3.7. In-line filtration onto cartridges. At each station, in-line filtration was carried out in the wet laboratory on seawater collected continuously at 2-m depth by the shipboard pump system (Table S1). Two polypropylene cartridges (Polycap HD), the first with a 20-µm pore size and the second with a 0.45-µm pore size, were mounted in series to recover the 0.45–20-µm and > 20-µm size fractions. Around 1000 L of seawater was filtered on the two cartridges at each station. The dissolved fraction (< 0.45 µm) was collected in 20-L plastic containers. These samples served for radionuclide analyses (^{137}Cs) (Radakovitch et al., in prep.).

2.3.8. Dilution experiments. At St1, St9, S15 and St19, seawater collected from the carousel bottles at 5-m depth and in the DCM was used to perform dilution experiments by means of a thermostatic incubation chamber (Table S1). These experiments were implemented to assess the phytoplankton production rates and microzooplankton grazing rates. At the same stations, the contents of the 200-µm Triple nets (vertical tows) were used to analyse the chlorophyll gut contents of mesozooplankton by fluorescence in order to estimate the impact of mesozooplankton grazing on large phytoplankton (i.e., nano- and micro-phytoplankton). These experiments and measurements served to determine the carbon fluxes and type and structure of the planktonic food webs (Medebb et al., in prep.).

2.3.9. Shipboard analyses. Unfiltered and 0.2-µm-filtered seawater collected from the carousel bottles at 5-m depth, in the DCM and at the other depths (profiles, OMZ) served for shipboard analyses of total and purgeable Hg using a Tekran® auto-analyser (model 2500),

consisting in purge and trap of volatilized Hg species followed by cold vapour atomic fluorescence spectrometry (CVAFS) detection (Table S1; Fig. S2m).

A part of the seawater collected continuously at 2-m depth by the shipboard pump system was subsampled and routed to a CytoSense® automated flow cytometer (CytoBuoy) installed in the dry laboratory. The CytoSense was employed to analyse (in terms of identification and abundance) individual or colonial phytoplankton cells sized between 0.8 and 800 µm. Cytometry measurements were carried out continuously at the different stations but also all along the transect (Table S1; Fig. S2l; Boudriga et al., 2022).

2.3.10. Atmospheric deposition. During the cruise, wet atmospheric deposition samples were collected using two rain collectors placed in PVC pipes that were fixed at the front of the ship (10 m above sea level). The collector for trace metal samples was composed of an acid pre-cleaned, metal-free plastic bottle and funnel (Fig. S2n). The collector for PAH samples was composed of a pre-combusted amber glass bottle and glass funnel (Table S1; Fig. S2o). Overall, six rainwater samples were collected (Table 3): two at St10 (Rains 1 and 2), one at St11 (Rain 3), one at St19 (Rain 4), one during the transit from off Djerba island to off Zarzis city (Rain 5, south of St19; Fig. 2a, b) (for both collectors), and one at St1 (Rain 6 only in the PAH collector). The "transit to Zarzis" sample was collected as a result of a dry deposition episode (intense Saharan dust event). In this case, ultra-pure water was used to rinse the plastic and glass funnels in order to retrieve all the dry fraction that had settled onto them. Atmospheric samples collected during the cruise were frozen and stored at –20 °C (for PAHs) or at 4 °C (for metals/metalloids), then filtered (at 0.2 or 0.7 µm) in the laboratory to separate dissolved and particulate phases before treatments and analyses. Atmospheric forecast bulletins were regularly sent to the on-board team to anticipate these rain events. Detailed information on the rain samples collected during the cruise can be found in Table 3.

Glass collectors were also set up in two ground stations located in the northern part (Marseille, France) and southern part (Sfax, Tunisia) of the Mediterranean basin (Fig. 2a; Fig. S2p) for sampling total (dry and wet) atmospheric deposition and running the subsequent PAH analyses. This sampling was done on a regular basis (bi-monthly, monthly, or daily in the case of strong rainfall events) from March 2019 to June 2020, i.e., before, during, and after the cruise (Poindron et al., in prep.).

2.3.11. On-vessel scientific equipment and continuous measurements.

Subsurface temperature and salinity were recorded continuously at high frequency all along the transect from flow-through pumped seawater at 2-m depth, using a thermosalinograph (TSG, SeaBird SBE 21). A weather station (Batos 1.1 D, Météo France) continuously recorded atmospheric parameters (temperature, wind, pressure, humidity, PAR).

2.4. The sequence of operations and main parameters analysed on the different size fractions

The typical sequence of at-sea/on-board operations conducted from the R/V *Antea* at each station is given in Table S2. The whole sequence of operations at each station lasted 48 h on average but varied depending on meteorological conditions encountered and occasional technical problems. The detailed sequence and timing of the main operations performed during the whole cruise are presented in Table S3, and the total number of operations completed is provided Table S4. Table S5 reports the time and depth of sampling (mostly in the DCM) at each station for the three main operations at sea: the water sampling with the carousel/Niskin and Go-Flo bottles, *in situ* filtration with the McLane pumps, and plankton sampling with the MultiNet. Table S6 summarises the main parameters analysed on the different size fractions (from < 0.2 to > 2000 µm) recovered from filtration and sieving after the collecting large amounts of plankton, particles, and water in the DCM and

surface/subsurface waters (0–5 m depth), i.e., 1) contaminants, with trace metals, organometals and metalloids (As, Cd, Cr, Cu, Fe, Hg, MeHg, Mn, Ni, Pb, Sb, Zn, etc.), organic contaminants (PAHs, PCBs, PBDEs, PFASs), radionuclides (^{137}Cs) and microplastics, 2) plankton biomass, size structure, taxonomy, cytometry, diversity, and pigment composition, and 3) biogeochemical parameters, including nutrients [$Si(OH)_4$, NO_3^-, NO_2^-, NH_4^+, PO_4^{3-}], TChl*a*, SPM, dissolved and particulate organic matter (POC, PON, DOC, a_{CDOM}), C and N isotopic ratios ($\delta^{13}C$, $\delta^{15}N$), and biochemical compounds (carbohydrates, proteins, lipids).

3. Environmental context during the cruise

3.1. Meteorological context

Atmospheric deposition is known to be an external source of metals and PAHs (Castro-Jimenez et al., 2012; Jordi et al., 2012; Desboeufs et al., 2022) as well as of nutrients (Guieu et al., 2020) for Mediterranean surface seawater. The cruise was conducted during the spring, when dust deposition events were commonplace in the Western Mediterranean (Guieu et al., 2020). During the cruise, the Aerosol Optical Depth (AOD) maps derived from the Spinning Enhanced Visible and InfraRed Imager (SEVIRI) satellite instrument (https://www.icare.univ-lille.fr/data-access/browse-images/geostationary-satellites/; Thieuleux et al., 2005) highlighted two dust transports with high AOD (> 0.8) through the Mediterranean Sea: one that occurred between 17 and 26 April 2019 (Fig. 4a; Fig. S6) and a second that occurred between 3 and 4 May 2019 (Fig. 5a; Fig. S7). These events were associated with significant cloud cover (Fig. 4b, 5b). The Non-hydrostatic Multiscale Model/Barcelona Supercomputing Centre (NMMB/BSC)-Dust model and NASCube (http://nascube.univ-lille1.fr/; Gonzales and

Briottet, 2017) confirmed the emission and export of dust plumes from North Africa to over the Western Mediterranean. The atmospheric dynamics and patterns of the first event are described in detail in Calidonna et al. (2020). This event was associated with a northward atmospheric flux loaded by dust emission from Algeria and southern Morocco. The second dust plume was transported from Algeria and Tunisia by north-eastward winds (not shown).

For the April event, dust plume transport was mainly associated with wet deposition from NMMB/BSC-Dust model forecasts, in agreement with the intensely cloudy conditions (Fig. 4c, d). The geographic range of dust deposition events covered a region from the Balearic basin to the Tyrrhenian Sea and then the Ligurian Sea (Fig. 4a-d), i.e., the vicinity of R/V's locations during St10 and St11 between 20 and 23 April and then on 25 April along the Western coastline of Sardinia (Table 1). The model predictions were confirmed by visual on-board observations of precipitations around and above the R/V's location, corresponding to the first three rain samples (Rains 1, 2 and 3) (Table 3). Note that wet dust deposition started from the afternoon of 22 April after the R/V's arrival on St10, thus ruling out a direct impact of dust deposition on the first cast completed at this station. However, rain events probably impacted surface waters over a large region around the R/V's location during St10 and St11.

For the event in May, NMMB/BSC-Dust model forecasts point mainly to dry dust deposition occurring between 3 and 4 May over the Gulf of Gabès and the Libyan coast (Fig. 5c, d). During this event, the R/V was at St19 in the southern Gulf of Gabès then in transit to Zarzis (Table 1; Table S3). Dry dust deposition was confirmed by visual observations of dusty sky and substantial deposited dust material on the decks of the R/V between 3 and 4 May. The Rain 5 sample was collected during this event (Table 3). The inflow of desert dust was also consistent with the highest temperatures and lowest pressures recorded by ship's permanent instrumentation (Fig. S8). It is therefore very likely that this event represented a supply of metal-bearing dust to the surface waters.

622 Outside of these desert dust transport periods, Hybrid Single-Particle Lagrangian
623 Integrated (HYSPLIT) back trajectories modelling showed that the air masses around the R/V
624 position came from Europe (not shown). Nevertheless, no intense pollution event was either
625 observed or predicted during the cruise from satellite or model outputs. Moreover, no
626 volcanic emissions from Etna were recorded during the cruise.
627
628 ### 3.2. Hydrological context
629 Subsurface (2-m depth) temperature gradually increased from north to south of the
630 transect, whereas subsurface salinity decreased from North to South but increased again at the
631 extreme south of the transect (Gulf of Gabès) (Fig. 6). The lowest subsurface temperatures (~
632 14.0 °C) were recorded in the Bay of Marseille, while the highest subsurface temperatures
633 (19.5 °C) were observed in the south of the Gulf of Gabès, near Djerba and Zarzis. The
634 highest subsurface salinity values were found in the Ligurian region (38.5) and the lowest
635 (37.1) in the northern Tunisian coastal waters, particularly in the Gulf of Tunis (Fig. 2a, 6;
636 Fig. S1). Because of the vast and contrasted area covered by the cruise, CTD profiles
637 displayed huge variability with depth in temperature and salinity and in TChl*a* and dissolved
638 O_2 concentrations between stations (Fig. 7, 8). Despite this high variability, some similarities
639 emerged. For the stations off French shores (St1–St4), temperature, salinity and TChl*a* values
640 over the water column ranged from 13.6–14.9 °C, 37.8–38.4 and 0.02–0.86 µg L^{-1},
641 respectively, with a slight decrease in temperature and a slight increase of salinity towards the
642 bottom (Fig. 7). Offshore stations (St9–St11) also showed a decrease in temperature and
643 increase of salinity with depth, but with a greater range of variation (compared to the stations
644 along the French coast) in terms of temperature (13.4–15.5 °C), salinity (37.3–38.7) and
645 TChl*a* concentrations (0.00–1.49 µg L^{-1}) with manifestly deeper thermoclines and haloclines
646 (Fig. 7, 8). TChl*a* concentrations were particularly high at St9 (Fig. 7). St11 was marked by a

647 significant increase in both temperature and salinity between 200 and 400 m followed by a
648 decrease between 400 and 430 m before remaining stable down to the bottom (Fig. 8).
649 Tunisian stations (St15–St19) showed higher water column temperatures (14.7–17.9 °C) and
650 lower salinities (37.2–37.8) compared to stations further north, in accordance with subsurface
651 data (Fig. 6), and lower TChl*a* concentrations (0.02–0.70 µg L^{-1}) compared to the
652 northernmost stations. At these Tunisian stations, thermoclines, haloclines and DCM were
653 located relatively deep in the water column, although St17 displayed much more
654 homogeneous profiles (Fig. 8).
655 T–S diagrams allowed us to identify the main water masses encountered at each station
656 (Fig. 9). At the northern stations (St1–St4) with temperatures of 13.6–14.9 °C and salinities of
657 37.8–38.4 over 0–150-m depths, we detected (modified) Atlantic Water (AW) coming mainly
658 from the Ligurian Sea and flowing along the continental slope with Ligurian-Provençal
659 current. These "resident" AW (RAW), which have been in the Mediterranean for a long time,
660 have been modified and are saltier (and warmer) than the AW that arrived more recently
661 through the Strait of Gibraltar (Millot and Taupier-Letage, 2005; Balbín et al., 2014). Moving
662 south, St9 was characterised by the presence of RAW over the depth 0–300 m and Levantine
663 Intermediate Water (LIW) over the depth 300–500 m (Fig. 9). LIW is formed in the Eastern
664 Mediterranean Basin by the combined effect of wintertime cooling and summertime
665 evaporation, leading to a warm (temperatures of 13.8–16 °C) and salty (salinities of 38.3–39)
666 intermediate layer that is visible over the whole Mediterranean Sea (Lascaratos et al., 1993;
667 Balbín et al., 2014; Margirier et al., 2020). Once formed, the LIW spreads throughout the
668 entire Eastern and Western Basins and can be identified through a salinity maximum at
669 between ~ 200 and 600-m depth in the Western Basin before it eventually flows out of the
670 Mediterranean Sea as one of the main components of Mediterranean outflow water (Ben
671 Ismail et al., 2012; Vargaz-Yanez et al., 2012). In addition, the presence of Western

672 Mediterranean Intermediate Water (WIW) was detected at St9 around 100-m depth with
673 temperatures of 13.2–13.9 °C and salinities of 38.4–38.6 (Fig. 7, 9). The WIW forms during
674 winter in the Northwestern Mediterranean Basin due to surface cooling of RAW and
675 intermediate convection (Salat and Font, 1987; Gasparini et al., 1999) and has been recorded
676 in the Algerian Basin by Benzohra and Millot (1995) and in the Sicily Channel by Ben Ismail
677 et al. (2012), flowing eastwards below the AW in the Algerian Current through the Channel
678 of Sardinia. The WIW is characterised by a relative minimum potential temperature located
679 between 100 and 200-m depth. The circulation of WIW has only been investigated in the
680 Algerian Basin, and there is speculation that it follows the same flow paths as the overlying
681 AW (Millot, 1999). St10 and St11 showed weak signature of the WIW and the presence of
682 marked LIW indicating a dominant influence of the northward advection of LIW rather than
683 winter cooling in the water column. The LIW water was well evident in St11, the closest
684 station to the Sardinia Channel (Fig. 8, 9). At the northernmost tip of the Tunisian coast, the
685 water temperature progressively increased and the salinity decreased, revealing the presence
686 of fresher or "new" AW (NAW) coming from the Algerian Basin. The water column arriving
687 at St15, located in the Gulf of Hammamet, was mostly made up of RAW and NAW with
688 temperatures of 14.8–17.5 °C and low salinities of 37.1–37.8 from surface to bottom. Moving
689 southward toward the Gulf of Gabès (GG), the temperature and salinity increased sharply to
690 reach 17.1 °C and 37.5 at St17 and 17.9 °C and 37.8 at St19 (Fig. 8, 9).
691
692 ### 3.3. Biogeochemical context
693 The analytical methods used to determine biogeochemical parameters presented in this
694 section are detailed in Text S1. Considering the whole cruise period, the average (over 32
695 days) surface TChl*a* concentration derived from satellite data was higher at St9 (~ 1 µg L^{-1})
696 than in the other stations (< 1 µg L^{-1}) (Fig. 10). The higher content of phytoplankton biomass

at St9 was also corroborated in the TChl*a* concentrations actually recorded during the cruise at 5-m depth, either from CTD measurements or analyses on discrete samples (with a significant correlation between both measurements: $r = 0.98$, $n = 10$, $p < 0.0001$; Table S7). In line with the discrete samples, the highest TChl*a* concentrations at 5-m depth were found at St9 (2.90 µg L^{-1}) followed by St4 (1.57 µg L^{-1}) and St1 (0.84 µg L^{-1}), while the lowest TChl*a* concentrations were observed at St17 (0.15 µg L^{-1}) and St15 (0.10 µg L^{-1}) (Table S7).

DCM was shallowest at St4 (13 m), St1 and St9 (20 m) and deepest at St10 (51 m), St2, St3 (53 m) and St15 (66 m) (Fig. 7, 8, 11a; Table S7). TChl*a* in the DCM followed a fairly similar pattern of distribution to TChl*a* at 5-m depth, with a significant correlation between both measures based on both CTD and discrete sample data ($r = 0.64–0.92$, $n = 10$, $p = 0.0001–0.048$). TChl*a* concentrations measured on discrete samples from the DCM were highest at St9 (1.54 µg L^{-1}), in line with the surface/subsurface TChl*a* data (Fig. 10). High TChl*a* concentrations were also recorded south of the Gulf of Gabès (at St19: 1.45 µg L^{-1}) (Fig. 11b; Table S7), even though at this station it was not really a DCM that was observed but rather a bottom-lying bead, as can often be observed for shallow coastal stations. St4 and St1 showed fairly high TChl*a* concentrations of 0.98 and 0.77 µg L^{-1}, respectively. The lowest TChl*a* concentrations in the DCM were found at St17 (0.21 µg L^{-1}), St2, and St11 (0.38 µg L^{-1}) (Fig. 11b; Table S7).

The North-to-South distribution of other biogeochemical parameters measured in the DCM presented interesting features. POC concentration had a fairly similar pattern of distribution to TChl*a*, with decreasing values from St1 to St3, a maximal value at St9 (156.4 µg L^{-1}), then a decrease up to St17, and finally a higher value at St19 (55.9 µg L^{-1}) (Fig. 11c; Table S7). $Si(OH)_4$ concentration followed much the same pattern but with an increase from St1 to St3 and a maximal value at both St9 and St19 (~ 2.00 µM) (Fig. 11d; Table S7). NO_3^- concentration increased from St1 to its peak at St3 (1.31 µM), was still high at St9 (0.96 µM),

and then decreased along to St17–St19 (Fig. 11e; Table S7). PO_4^{3-} concentration was particularly high at St3 (0.31 µM) and St19 (0.55 µM) (Fig. 11f; Table S7). Finally, DOC concentration and a_{CDOM} decreased from St1 to St9 or St10 then increased up to St19 where they reached maximal values (76.2 µM and 2.05 m^{-1}, respectively) (Fig. 11g, h; Table S7).

Principal component analysis (PCA) based on the Pearson's correlation matrix was applied on these biogeochemical parameters recorded in the DCM at each station (Fig. 12). The first principal component (PC1), which explained 47% of total variance within samples, was mainly driven by PO_4^{3-}, DOC, a_{CDOM}, and to a lesser extent TChl*a* and $Si(OH)_4$. The second principal component (PC2), which accounted for 34% of total variance, was driven by POC, NO_3^-, TChl*a*, and $Si(OH)_4$. Four groups of samples (stations) emerged from this PCA: 1) St2, St3, St4, St10, characterised by moderate concentrations of nutrients and TChl*a* and a low organic matter content; 2) St1, St11, St15, St17, with the lowest concentrations in nutrients and TChl*a* (except St1); 3) St9, which showed the highest in $Si(OH)_4$, NO_3^-, TChl*a* and POC concentrations, and the lowest PO_4^{3-} and DOM contents; 4) St19, which showed the highest concentrations in $Si(OH)_4$, TChl*a* (equivalent to those of St9), PO_4^{3-} and DOM as well as high POC and low NO_3^- concentrations (Fig. 12).

Overall, the levels of TChl*a*, nutrients and other biogeochemical parameters observed along the North-South transect in the subsurface waters and DCM in spring 2019 during the MERITE-HIPPOCAMPE cruise are consistent with previous observations in the Mediterranean Sea (The Mermex Group, 2011; Salgado-Hernanz et al., 2019; Guieu et al., 2020; Marañón et al., 2021). The TChl*a* levels in the different stations were also consistent with their positioning in terms of bloom-condition areas and consensus regions defined by D'Ortenzio and d'Alcalà (2009) and Ayata et al. (2018). TChl*a* concentrations tended to be higher at stations located north of the North Balearic front (St1–St4, St9) than stations located south (St10, St11, St15, St17, St19).

Interestingly, two stations, St9 and St19, clearly stood apart from the others in terms of biogeochemical content (Fig. 11, 12). St9 was situated at the boundary of the Ligurian consensus region, in the wintertime deep convection area. Time-series of water temperature recorded at different depths at the LION mooring (42° 02' N, 4° 40' E) highlighted a deepening of the mixed layer depth and thus the convection process down to 1500-m depth within the Ligurian area in early February 2019 (Fig. S9). In late March 2019, the end of the convection process induced the occurrence of an intense phytoplankton bloom in the same area (Fig. S9). This illustrates the fact that 2019 was a relatively convective and productive year (Margirier et al., 2020; Bosse et al., 2022), and that St9, located at the border of this convective and productive zone, still presented high concentrations of TChl*a*, POC and some nutrients in the May 2019 sampling period.

The high levels of TChl*a*, $Si(OH)_4$, PO_4^{3-}, DOM, and POC encountered at St19 south of the Gulf of Gabès is probably related to the Saharan dust deposition event (see section 3.1), but the effect of sediment resuspension cannot be excluded due to high wind speeds during this period (Fig. S8). In the Gulf of Gabès, TChl*a* concentrations can reach > 1 µg L^{-1} close to the coast of Djerba and Kerkennah Islands during the spring season (Bel Hassen et al., 2009). The Gulf of Gabès is known to be regularly submitted to Saharan dust deposition (Béjaoui et al., 2019). This Saharan dust, enriched in phosphorus, has been shown to induce phytoplankton blooms in the Gulf (Hamza et al., 2016; Béjaoui et al., 2019), and as described above, intense Saharan dust deposition events occurred in this area during the cruise, for which we collected on-board rain and particle samples (Table 3; Fig. 5; Fig. S7, S8). Furthermore, in this shallow ecosystem submitted to strong tides and resulting currents, disturbance and resuspension of sediments could release elements such as nutrients and organic matter into the water column, which in turn may stimulate planktonic activity (Bel Hassen et al., 2009; Fourati et al., 2018; Zouch et al., 2018).

4. Overview of the types of articles produced through the cruise

Fig. 13 shows the types of articles that are a part of this special issue in the frame of the MERITE-HIPPOCAMPE cruise. There are a series of articles concerning the transfer and accumulation of contaminants in planktonic food webs in the DCM but also in surface/subsurface waters. These articles present: 1) contaminant concentrations in the different planktonic/particulate size fractions and, for several of them, in the dissolved phase of water (see Table S6 for the size fractions–contaminant analysis correspondence), and 2) their resulting factors of bioconcentration, bioaccumulation or food accumulation. The contaminants investigated are trace metals/metalloids (Cr, Mn, Fe, Co, Ni, Cu, Zn, As, Se, Mo, Ag, Cd, Sb, Pb…) (Chifflet et al., 2023), with a focus on Cu and Zn isotopes (Chifflet et al., 2022), Hg and MeHg (Tesán Onrubia et al., in prep.), PAHs (Guigue et al., in prep.), PCBs, PBDEs, PFASs (Tronczynski et al., in prep.), and radionuclides (^{137}Cs) (Radakovitch et al., in prep.). Another work will treat of the abundance and composition of microplastics in both surface waters and the DCM (Fig. 13).

There are also a series of articles dealing with the composition and structure of planktonic food webs. Indeed, the paper by Tesán Onrubia et al. (2023) on the stable C and N isotopes (δ^{13}C, δ^{15}N) and biochemical content (lipids, carbohydrates, proteins) of the different planktonic size fractions serves to highlight the structure of planktonic food webs and the transfer of organic matter within them, and to assess the factors of trophic accumulation used in the contaminant-related papers. Moreover, several articles use the cytometry and taxonomy/microscope analyses, imaging (zooscan, flowcam), optical *in situ* measurements (LOPC, LISST-HOLO) and/or 16S and 18S rRNA high-throughput sequencing analyses to

cover the abundance, biomass, distribution, size structure, and composition/diversity of the following planktonic groups, mostly for the DCM but also for surface/subsurface waters or even within the 0–200-m depth layer (see Table S6 for the correspondence with size fractions): pico-, nano- and micro-phytoplankton (Boudriga et al., 2022; Bellaaj Zouari et al., in prep.), micro- and meso-zooplankton and their biomass ratio with detritus (Fierro-González et al., 2023), as well as free-living and plankton-associated bacterioplankton (heterotrophic prokaryotes) (Bellaaj Zouari et al., in prep.; Quéméneur et al., in prep.), and nano- and micro-zooplankton related to the microbial loop (Bellaaj Zouari et al., in prep.). In addition, a complementary paper proposes a methodological approach for the study of the microbiota associated with plankton (Cabrol et al., in prep.). Also, the effect of the Saharan dust deposition event on pico- and nano-phytoplankton community in the south of Gabès is covered by Boudriga et al. (in prep.). Overall, these articles will allow us to understand which planktonic groups are present and how they influence/participate in transfers of contaminants within planktonic networks. Our understanding of the contaminant transfer processes at work within planktonic food webs is also enhanced by the dilution experiments and the subsequent determination of phytoplankton production rates and micro- and meso-zooplankton grazing rates (Meddeb et al., in prep.) (Fig. 13), as well as the grazing and excretion rates estimated from the zooplankton size-structure according to allometric relationships allowing an estimation of grazing pressure and nutrient recycling by the metazooplankton (Fierro-González et al., 2023).

Looking beyond plankton, there is one article dedicated to $\delta^{13}C$ and $\delta^{15}N$ stable isotopes and concentrations of Hg, PAHs and PCBs in small pelagic fishes collected in Tunisian waters (Lajnef et al., in prep.). This study should provide valuable pointers to help establish a link between the contamination of plankton and the contamination of higher trophic levels. The concentrations of trace metals and PAHs in wet (rain) atmospheric deposition samples

collected during the cruise and on land is investigated to assess the role of dry/wet atmospheric deposition as a source of contaminants in surface marine waters (Poindron et al., in prep.). Finally, the overall transport patterns and hydrodynamic context of the cruise using modelling and satellite data, and their potential implication for contaminant origin and distribution are addressed by Rwawi et al. (in prep.) (Fig. 13).

Data availability

All data from the MERITE-HIPPOCAMPE cruise (https://doi.org/10.17600/18000900; Tedetti and Tronczynski, 2019) is stored in the MISTRALS-SEDOO database (https://mistrals.sedoo.fr/MERITE/) and will be made publicly accessible once all the articles related to the cruise are published in the present special issue. In the meantime, data can be obtained upon request from the corresponding author. In addition, navigation data and CTD profiles from the MERITE-HIPPOCAMPE cruise are available *via* the IFREMER/SISMER database (https://data.ifremer.fr/SISMER).

Author contribution statement

All the authors participated in the MERITE-HIPPOCAMPE project and design of the manuscript.

Conception and design of study: M.T., J.T., F.C., M.P., S.B.I., C.S., M.B.H., K.D., S.C., A.B.Z., D.B., A.B., C.B.-P., N.B., L.C., C.C., L.C., M.N.D.Y., A.D., J.-C.D., C.G., L.G., A.H., L.-E.H.-B., S.J., J.K., B.M., O.P., M.Q., O.R., A.S.H., M.T., N.Z., C.G.

Acquisition of data: M.T., J.T., F.C., M.P., S.B.I., M.B.H., K.D., S.C., A.B.Z., M.A., S.A., L.B.A., N.B., I.B., A.B., N.B., L.C., T. de G.-T., M.F., F.G., L.G., J.K., N.M.B., D.M., J.-C.M., M.M., M.Q., O.R., C.R., A.S.H., J.A.T.O., B.T., M.T., N.Z.

Analysis and/or interpretation of data: M.T., J.T., F.C., M.P., S.B.I., M M.B.H., K.D., C.P., S.C., A.B.Z., S.A., D.B., L.B.A, I.B., A.B., C.B.-P., N.B., L.C., C.C., L.C., S.C., A.D., B.E., P.F.-G., N.G., F.G., C.G., L.G., A.H., L.-E.H.-B., S.J., J.K., R.L., N.M.B, P.L.M., A.B., M.M., B.M., M.Q., O.R., P.R., V.R., C.R., A.S.H., J.A.T.O., B.T., M.T., N.Z.

Drafting the manuscript: M.T., J.T., F.C., M.P., S.B.I., K.D., C.P., S.C., P.L.M., A.B.

Revising/editing the manuscript: J.T., F.C., M.P., C.S., M.B.H., K.D., C.P., A.B.Z., M.A., S.A., D.B., L.B.A., N.B., I.B., A.B., C.B.-P., N.B., L.C., C.C., L.C., S.C., M.N.D.Y., T. de G.-T., A.D., J.-C.D., B.E., P.F.-G., M.F., N.G., F.G., C.G., L.G., A.H., L.-E.H.-B., S.J., J.K., R.L., N.M.B., D.M., A.B., J.-C.M., M.M., B.M., O.P., M.Q., O.R., P.R., C.R., V.R., C.R., A.S.H., J.A.T.O., B.T., M.T., N.Z.

Project administration and funding acquisition: M.T., J.T., F.C., M.P., K.D., C.S.

Acknowledgments

The MERITE-HIPPOCAMPE project was initiated and funded by the cross-disciplinary *Pollution & Contaminants* axis of the CNRS-INSU MISTRALS program (joint action of the MERMEX-MERITE and CHARMEX subprograms). The project also received financial support from the IRD French-Tunisian International Joint Laboratory (LMI) COSYS-Med. The MERITE-HIPPOCAMPE cruise was organised and supported by the French Oceanographic Fleet (FOF), CNRS/INSU, IFREMER, IRD, the Tunisian Ministry of Agriculture, Water Resources and Fisheries, and the Tunisian Ministry of Higher Education and Scientific Research. The project also benefited from additional funding by IFREMER, by

870 the MIO Action Sud and Transverse Axis programs (CONTAM Transverse Axis), by the IRD
871 Ocean Department, and by the CONTAMPUMP project, funded by the French National
872 Research Agency (ANR) (ANR JCJC #19-CE34-0001-01). It was also supported by the
873 Chemical and Physical Properties of the Atmosphere (CaPPA) project, funded by the ANR
874 through the Programme d'Investissement d'Avenir (PIA) under contract ANR-11-LABX-
875 0005-01, and by the Regional Council Nord-Pas de Calais and the European Funds for
876 Regional Economic Development (FEDER). We are grateful to the captains and crew of the
877 R/V *Antea* for their help and assistance during the cruise, as well as to the captain and crew of
878 the R/V *Hannibal* (INSTM, Tunisia) for sampling small pelagic fishes in the Tunisian waters.
879 We also thank the captain and crew of the R/V *Antédon 2* for the pre-HIPPOCAMPE cruise
880 performed in the Bay of Marseille in 2018. IFREMER-FOF and Genavir teams provided
881 valuable technical and administrative support for the preparation and conduct of the cruise.
882 We warmly thank P. Vert, F. André and A. Miere from Observatoire Midi-Pyrénées/SEDOO
883 for the implementation of the HIPPOCAMPE Operation Centre (http://hippoc.sedoo.fr/) and
884 the MERITE-HIPPOCAMPE database (https://mistrals.sedoo.fr/MERITE/). We also thank F.
885 Dulac (LSCE) for his contribution in the early phases of the project. We thank E. de Saint-
886 Léger and F. Perault (DT-INSU, Brest) for provisioning the *in situ* McLane pumps with
887 sequential filtration units, and A. Smirnov (NASA Goddard Space Flight Centre) for
888 provisioning the Microtops sunphotometer. The IRD's representation in Tunisia, the French
889 Institute of Tunisia, and INSTM provided valuable logistics and/or financial assistance to help
890 prepare the cruise, and CNRS-INSU, IFREMER, IRD, IRSN and MIO communications and
891 outreach divisions helped promote the campaign. We are grateful to the Station Marine
892 d'Endoume (OSU Institut Pythéas, Aix-Marseille Université, CNRS) and to the INSTM for
893 providing the facilities to host the atmospheric deposition collectors in Marseille and Sfax.
894 We thank L. Casalot (MIO) and the IRD for helpful support on implementing the "Accès et

partage des avantages découlant de l'utilisation des ressources génétiques et des connaissances traditionnelles associées" (APA) procedure. Various MIO platforms also provided valuable support: the Service Atmosphère-Mer (SAM), for preparation and management of the embarked material, the Plateforme Analytique de Chimie des Environnements Marins (PACEM platform) for various chemical analyses, the Platform Microscopie et Imagerie (MIM platform) for plankton analyses, and the Plateforme Régionale de Cytométrie pour la Microbiologie (PRECYM platform) for cytometric analyses. L. Gouriou (IFREMER, LER-AR Arcachon) ran HPLC analyses of the pigments. I. Fronval and V. Riffault (IMT NE) performed the analyses of PAHs in atmospheric deposition and contributed to data interpretation. We used imagery taken from the NASA Worldview application (https://worldview.earthdata.nasa.gov), which is part of the NASA Earth Observing System Data and Information System (EOSDIS). Data and/or images from the NMMB/BSC-Dust or BSC-DREAM8b model were produced by the Barcelona Supercomputing Centre (http://www.bsc.es/ess/bsc-dust-daily-forecast/). The average surface Chl*a* image was obtained from EU Copernicus Marine Service Information (CMEMS; https://marine.copernicus.eu/). This paper and special issue are dedicated to our friend and colleague, Cédric Garnier, who passed away in 2018. Cédric was a deeply-involved and very active member of the MERMEX-MERITE program, and was part of the team that initiated and promoted the MERITE-HIPPOCAMPE cruise project. Finally, we are grateful to two anonymous reviewers for their helpful and constructive comments and corrections.

Supplementary information

Supplementary material related to this article is available online at: xxx

References

Alcaraz, M., Calbet, A., 2003. Zooplankton Ecology. Marine Ecology, pp. 16.

Alekseenko, E., Thouvenin, B., Tronczyński, J., Carlotti, F., Garreau, P., Tixier, C., Baklouti, M., 2018. Modeling of PCB trophic transfer in the Gulf of Lions; 3D coupled model application. Marine Pollution Bulletin, 128, 140–155. doi: 10.1016/j.marpolbul.2018.01.008

Ayata, S.D., Irisson, J.O., Aubert, A., Berline, L., Dutay, J.C., Mayot, N., Nieblas, A.E., D'Ortenzio, F., Palmieri, J., Reygondeau, G., Rossi, V., Guieu, C., 2018. Regionalisation of the Mediterranean basin, a MERMEX synthesis. Progress in Oceanography, 163, 7–20. doi: 10.1016/j.pocean.2017.09.016

Balbín, R., López-Jurado, J., Flexas, M., Reglero, P., Vélez-Velchí, P., González-Pola, C., Rodríguez, J., García, A., Alemanya, F., 2014. Interannual variability of the early summer circulation around the balearic islands: Driving factors and potential effects on the marine ecosystem. Journal of Marine Systems, 138, 70–81. doi: 10.1016/j.jmarsys.2013.07.004

Barhoumi, B., Castro-Jiménez, J., Guigue, C., Goutx, M., Sempéré, R., Derouiche, A., Achour, A., Touil, S., Driss, M.R., Tedetti, M., 2018. Levels and risk assessment of hydrocarbons and organochlorines in aerosols from a north African coastal city (Bizerte, Tunisia). Environmental Pollution, 240, 422–431. doi: 10.1016/j.envpol.2018.04.109

Barral, Q.B., Zakardjian, B., Dumas, F., Garreau, P., Testor, P., Beuvier, J., 2021. Characterization of fronts in the Western Mediterranean with a special focus on the North Balearic Front. Progress in Oceanography, 197, 102636. doi: 10.1016/j.pocean.2021.102636

Barrier, N., Petrenko, A.A., Ourmières, Y., 2016. Strong intrusions of the Northern Mediterranean Current on the eastern Gulf of Lion: insights from in-situ observations and

high resolution numerical modelling. Ocean Dynamics, 66, 313–327. doi: 10.1007/s10236-016-0921-7

Béjaoui, B., Ben Ismail, S., Othmani, A., Ben Abdallah-Ben Hadj Hamida, O., Chevalier, C., Feki-Sahnoun, W., Harzallah, A., Ben Hadj Hamida, N., Bouaziz, R., Dahech, S., Diaz, F., Tounsi, K., Sammari, C., Pagano, M., Bel Hassen, M., 2019. Synthesis review of the Gulf of Gabes (eastern Mediterranean Sea, Tunisia): morphological, climatic, physical oceanographic, biogeochemical and fisheries features. Estuarine, Coastal and Shelf Science, 219, 395–408. doi: 10.1016/j.ecss.2019.01.006

Bel Hassen, M., Hamza, A., Drira, Z., Zouari, A., Akrout, F., Messaoudi, S., Aleya, L., Ayadi, H., 2009. Phytoplankton-pigment signatures and their relationship to spring summer stratification in the Gulf of Gabes. Estuarine, Coastal and Shelf Science, 83, 296–306. doi: 10.1016/j.ecss.2009.04.002

Ben Ismail, S., Sammari, C., Gasparini, G.P., Béranger, K., Brahim, M., Aleya, L., 2012. Water masses exchanged through the Channel of Sicily: evidence for the presence of new water masses on the Tunisian side of the Channel. Deep Sea Research Part I, 63, 65–81. doi: 10.1016/j.dsr.2011.12.009

Benzohra, M., Millot, C., 1995. Characteristics and circulation of the surface and intermediate water masses off Algeria. Deep-Sea Research Part I, 42, 1803–1830. doi: 10.1016/0967-0637(95)00043-6

Berline, L., Rammou, A., Doglioli, A., Molcard, A., Petrenko, A., 2014. A connectivity based ecoregionalization of the Mediterranean Sea. PLoS ONE, 9, e111978. doi: 10.1371/journal.pone.0111978

Berrojalbiz, N., Dachs, J., Ojeda, M.J., Valle, M.C., Castro-Jimenez, J., Wollgast, J., Ghiani, M., Hanke, G., Zaldivar, J.M., 2011. Biogeochemical and physical controls on concentrations of polycyclic aromatic hydrocarbons in water and plankton of the

969 Mediterranean and Black Seas. Global Biogeochemical Cycles, 25, GB4003.
970 doi:10.1029/2010GB003775, 2011
971 Bishop, J.K.B., Lam, P.J., Wood, T.J., 2012. Getting good particles: Accurate sampling of
972 particles by large volume in-situ filtration. Limnology and Oceanography: Methods, 10,
973 681–710. doi: 10.4319/lom.2012.10.681
974 Bishop, J.K.B., Wood, T.J., 2008. Particulate matter chemistry and dynamics in the twilight
975 zone at VERTIGO ALOHA and K2 sites. Deep Sea Research I, 55, 1684–1706. doi:
976 10.1016/j.dsr.2008.07.012
977 Bodiguel, X., Loizeau, V., Le Guellec, A.-M., Roupsard, F., Philippon, X., Mellon-Duval, C.,
978 2009. Influence of sex, maturity and reproduction on PCB and p,p′DDE concentrations and
979 repartitions in the European hake (*Merluccius merluccius*, *L.*) from the Gulf of Lions
980 (N.W. Mediterranean). Science of the Total Environment, 408, 304–311. doi:
981 10.1016/j.scitotenv.2009.10.004
982 Bosse, A., Testor, P., Coppola L., Bretel, P., Dausse, D., Durrieu de Madron, X., Houpert, L.,
983 Labaste, M., Legoff, H., Mortier, L., D'Ortenzio, F., 2022. LION observatory data.
984 SEANOE. doi: 10.17882/44411
985 Boudriga, I., Thyssen, M., Zouari, A., Garcia, N., Tedetti, M., Bel Hassen, M., 2022.
986 Ultraphytoplankton community structure in subsurface waters along a North-South
987 Mediterranean transect. Marine Pollution Bulletin, 182, 113977. doi:
988 10.1016/j.marpolbul.2022.113977
989 Calidonna, C.R., Avolio, E., Gullì, D., Ammoscato, I., De Pino, M., Donateo, A., Lo Feudo,
990 T., 2020. Five Years of Dust Episodes at the Southern Italy GAW Regional Coastal
991 Mediterranean Observatory: Multisensors and Modeling Analysis. Atmosphere, 11, 456.
992 doi: 10.3390/atmos11050456

993 Casal, P., González-Gaya, B., Zhang, Y., Reardon, A.J.F., Martin, J.W., Jiménez, B., Dachs,
994 J., 2017. Accumulation of perfluoroalkylated substances in oceanic plankton.
995 Environmental Science and Technology, 51, 2766–2775. doi: 10.1021/acs.est.6b05821
996 Castro-Jiménez, J., Bănaru, D., Chen, C.-T., Jiménez, B., Muñoz-Arnanz, J., Deviller, G.,
997 Sempéré, R., 2021. Persistent organic pollutants burden, trophic magnification and risk in a
998 pelagic food web from coastal NW Mediterranean Sea. Environmental Science and
999 Technology, 55, 9557–9568. doi: 10.1021/acs.est.1c00904
1000 Castro-Jiménez, J., Barhoumi, B., Paluselli, A., Tedetti, M., Jiménez, B., Muñoz-Arnanz, J.,
1001 Wortham, H., Driss, M.R., Sempéré, R., 2017. Occurrence, loading and exposure of
1002 atmospheric particle-bound POPs at the African and European edges of the western
1003 Mediterranean Sea. Environmental Science and Technology, 51, 13180–13189. doi:
1004 10.1021/acs.est.7b04614
1005 Castro-Jiménez, J., Berrojalbiz, N., Wollgast, J., Dachs, J., 2012. Polycyclic aromatic
1006 hydrocarbons (PAHs) in the Mediterranean Sea: Atmospheric occurrence, deposition and
1007 decoupling with settling fluxes in the water column. Environmental Pollution, 166, 40–47.
1008 doi: 10.1016/j.envpol.2012.03.003
1009 Chifflet, S., Briant, N., Freydier, R., Araújo, D.F., Quéméneur, M., Zouch, H., Bellaaj-Zouari,
1010 A., Carlotti, F., Tedetti, M., 2022. Isotopic compositions of copper and zinc in plankton
1011 from the Mediterranean Sea (MERITE-HIPPOCAMPE campaign): Tracing trophic
1012 transfer and geogenic inputs. Marine Pollution Bulletin, 185, 114315. doi:
1013 10.1016/j.marpolbul.2022.114315
1014 Chifflet, S., Briant, N., Tesán-Onrubia, J.A., Zaaboub, N., Amri, S., Radakovitch, O., Bãnaru,
1015 D., Tedetti, M., 2023. Distribution and accumulation of metals and metalloids in
1016 planktonic food webs of the Mediterranean Sea (MERITE-HIPPOCAMPE campaign).
1017 Marine Pollution Bulletin, 186, 114384. doi: 10.1016/j.marpolbul.2022.114384

1018 Chouvelon, T., Cresson, P., Bouchoucha, M., Brach-Papa, C., Bustamante, P., Crochet, S.,
1019 Marco-Miralles, F., Thomas, B., Knoery, J., 2018. Oligotrophy as a major driver of
1020 mercury bioaccumulation in medium-to high-trophic level consumers: a marine ecosystem-
1021 comparative study. Environmental Pollution, 233, 844–854. doi:
1022 10.1016/j.envpol.2017.11.015
1023 Chouvelon, T., Strady, E., Harmelin-Vivien, M., Radakovitch, O., Brach-Papa, C., Crochet,
1024 S., Knoery, J., Rozuel, E., Thomas, B., Tronczynski, J., Chiffoleau, J.F., 2019. Patterns of
1025 trace metal bioaccumulation and trophic transfer in a phytoplankton-zooplankton-small
1026 pelagic fish marine food web, Marine Pollution Bulletin, 146, 1013–1030. doi:
1027 10.1016/j.marpolbul.2019.07.047
1028 Cossa, D., Coquery, M., 2005. The Mediterranean mercury anomaly, a geochemical or a
1029 biological issue. In: Saliot, A. (Ed.), The Mediterranean Sea. Handbook of Environmental
1030 Chemistry, pp. 177–208
1031 Cossa, D., Knoery, J., Bănaru, D., Harmelin-Vivien, M., Sonke, J.E., Hedgecock, I.M., Bravo,
1032 A.G., Rosati, G., Canu, D., Horvat, M., Sprovieri, F., Pirrone, N., Heimbürger-Boavida,
1033 L.E., 2022. Mediterranean Mercury Assessment 2022: An Updated Budget, Health
1034 Consequences, and Research Perspectives. Environmental Science and Technology, 56,
1035 3840–3862. doi: 10.1021/acs.est.1c03044
1036 D'Ortenzio, F., d'Alcalà, M.R., 2009. On the trophic regimes of the Mediterranean Sea: a
1037 satellite analysis. Biogeosciences, 6, 139–148. doi: 10.5194/bg-6-139-2009
1038 Dachs, J., Lohmann, R., Ockenden, W.A., Mejanelle, L., Eisenreich, S.J., Jones, K.C., 2002.
1039 Oceanic biogeochemical controls on global dynamics of persistent organic pollutants.
1040 Environmental Science and Technology, 36, 4229–4237. doi: 10.1021/es025724k

1041 Dachs, J., Méjanelle, L., 2010. Organic Pollutants in Coastal Waters, Sediments, and Biota: A
1042 Relevant Driver for Ecosystems During the Anthropocene? Estuaries and Coasts, 33, 1–14.
1043 doi: 10.1007/s12237-009-9255-8
1044 Desboeufs, K., Fu, F., Bressac, M., Tovar-Sánchez, A., Triquet, S., Doussin, J.-F., Giorio, C.,
1045 Chazette, P., Disnaquet, J., Feron, A., Formenti, P., Maisonneuve, F., Rodríguez-Romero,
1046 A., Zapf, P., Dulac, F., Guieu, C., 2022. Wet deposition in the remote western and central
1047 Mediterranean as a source of trace metals to surface seawater. Atmospheric Chemistry and
1048 Physics, 22, 2309–2332, https://doi.org/10.5194/acp-22-2309-2022.
1049 Ding, Q., Gong, X., Jin, M., Yao, X., Zhang, L., Zhao, Z., 2021. The biological pump effects
1050 of phytoplankton on the occurrence and benthic bioaccumulation of hydrophobic organic
1051 contaminants (HOCs) in a hypereutrophic lake. Ecotoxicology and Environmental Safety,
1052 213, 112017. doi: 10.1016/j.ecoenv.2021.112017
1053 Duran, R., Cravo-Laureau, C., 2016. Role of environmental factors and microorganisms in
1054 determining the fate of polycyclic aromatic hydrocarbons in the marine environment.
1055 FEMS Microbiology Reviews, 40, 814–830. doi: 10.1093/femsre/fuw031
1056 El Hourany, R., Abboud-Abi Saab, M., Faour, G., Mejia, C., Crépon, M., Thiria, S., 2019.
1057 Phytoplankton diversity in the Mediterranean Sea from satellite data using self-organizing
1058 maps. Journal of Geophysical Research Oceans, 124, 5827–5843. doi:
1059 10.1029/2019JC015131
1060 Elbaz-Poulichet, F., Morley, N.H., Beckers, J.-M., Nomerange, P., 2001. Metal fluxes through
1061 the Strait of Gibraltar: the influence of the Tinto and Odiel rivers (SW Spain). Marine
1062 Chemistry, 73, 93–213. doi: 10.1016/S0304-4203(00)00106-7
1063 Everaert, G., De Laender, F., Goethals, P.L.M., Janssen, C.R., 2015. Multidecadal field data
1064 Support intimate links between phytoplankton dynamics and PCB concentrations in marine

1065 sediments and biota. Environmental Sciences and Technology, 49, 8704–8711. doi:
1066 10.1021/acs.est.5b01159
1067 Fan, C.-W., Reinfelder, J.R., 2003. Phenanthrene Accumulation Kinetics in Marine Diatoms.
1068 Environmental Science and Technology, 37, 3405−3412. doi: 10.1021/es026367g
1069 Fierro-González, P., Pagano, M., Guilloux, L., Makhlouf Belkahia, N., Tedetti, M., Carlotti,
1070 F., 2023. Zooplankton biomass, size structure, and associated metabolic fluxes with focus
1071 on its roles at the chlorophyll maximum layer during the plankton-contaminant MERITE-
1072 HIPPOCAMPE cruise. Submitted to this special issue.
1073 Fourati, R., Tedetti, M., Guigue, C., Goutx, M., Garcia, N., Zaghden, H., Sayadi, S., Elleuch,
1074 B., 2018. Sources and spatial distribution of dissolved aliphatic and polycyclic aromatic
1075 hydrocarbons in surface coastal waters from the Gulf of Gabès (Tunisia, Southern
1076 Mediterranean Sea). Progress in Oceanography, 163, 232−247. doi:
1077 10.1016/j.pocean.2017.02.001
1078 Frouin, H., Dangerfield, N., Macdonald, R.W., Galbraith, M., Crewe, N., Shaw, P., Mackas,
1079 D., Ross, P.S., 2013. Partitioning and bioaccumulation of PCBs and PBDEs in marine
1080 plankton from the Strait of Georgia, British Columbia, Canada. Progress in Oceanography,
1081 115, 65–75. doi: 10.1016/j.pocean.2013.05.023
1082 Galbán-Malagón, C., Berrojalbiz, N., Ojeda, M.J., Dachs, J., 2012. The oceanic biological
1083 pump modulates the atmospheric transport of persistent organic pollutants to the Arctic.
1084 Nature Communications, 3, 862. doi: 10.1038/ncomms1858
1085 Gasparini, G.P., Zodiatis, G., Astraldi, M., Galli, C., Sparnocchia, S., 1999. Winter
1086 Intermediate Water lenses in the Ligurian Sea. Journal of Marine Systems, 20, 319–332.
1087 doi: 10.1016/s0924-7963(98)00089-x
1088 Gonzalez, L., Briottet, X., 2017. North Africa and Saudi Arabia day/night sandstorm survey
1089 (NASCube). Remote Sensing, 9, 896. doi: 10.3390/rs9090896

González-Gaya, B., Martínez-Varela, A., Vila-Costa, M., Casal, P., Cerro-Gálvez, E., Berrojalbiz, N., Lundin, D., Vidal, M., Mompean, C., Bode, A., Jiménez, B., Dachs, J., 2019. Biodegradation as an important sink of aromatic hydrocarbons in the oceans. Nature Geosciences, 12, 119–125. doi: 10.1038/s41561-018-0285-3

Guieu, C., D'Ortenzio, F., Dulac, F., Taillandier, V., Doglioli, A., Petrenko, A., Barrillon, S., Mallet, M., Nabat, P., Desboeufs, K., 2020. Introduction: Process studies at the air–sea interface after atmospheric deposition in the Mediterranean Sea – objectives and strategy of the PEACETIME oceanographic campaign (May–June 2017). Biogeosciences, 17, 5563–5585. doi: 10.5194/bg-17-5563-2020, 2020

Guigue, C., Tedetti, M., Ferretto, N., Garcia, N., Méjanelle, L., Goutx, M., 2014. Spatial and seasonal variabilities of dissolved hydrocarbons in surface waters from the Northwestern Mediterranean Sea: Results from one year intensive sampling. Science of the Total Environment, 466–467, 650–662. doi: 10.1016/j.scitotenv.2013.07.082

Hamza, I., Feki, W., Hamza, A., Bel Hassen, M., 2016. Long term characterization of *Trichodesmium erythraeum* blooms in Gabes Gulf (Tunisia). Continental Shelf Research, 124, 95–103. doi: 10.1016/j.csr.2016.05.007

Harmelin-Vivien, M., Cossa, D., Crochet, S., Bănaru, D., Letourneur, Y., Mellon-Duval, C., 2009. Difference of mercury bioaccumulation in red mullets from the north-western Mediterranean and Black seas. Marine Pollution Bulletin, 58, 679–685. doi: 10.1016/j.marpolbul.2009.01.004

Heimbürger, L.E., Cossa, D., Marty, J.C., Migon, C., Averty, B., Dufour, A., Ras, J., 2010. Methylmercury distributions in relation to the presence of nano and picophytoplankton in an oceanic water column (Ligurian Sea, North-western Mediterranean). Geochimica Cosmochimica Acta, 74, 5549–5559. doi: 10.1016/j.gca.2010.06.036

1114 Heimbürger, L.E., Migon, C., Cossa, D., 2011. Impact of atmospheric deposition of
1115 anthropogenic and natural trace metals on Northwestern Mediterranean surface waters: A
1116 box model assessment. Environmental Pollution, 159, 1629–1634. doi:
1117 10.1016/j.envpol.2011.02.046.
1118 Hinrichsen, D., 1990. Our common seas: Coasts in crisis. Earthscan Publications, London, in
1119 association with United Nations Environment Programme, Nairobi, 184 pp.
1120 Hunt, B.P.V., Carlotti, F., Donoso, K., Pagano, M., D'Ortenzio, F., Taillandier, V., Conan, P.,
1121 2017. Trophic pathways of phytoplankton size classes through the zooplankton food web
1122 over the spring transition period in the north-west Mediterranean Sea. Journal of
1123 Geophysical Research Oceans, 122, 6309–6324. doi:10.1002/2016JC012658
1124 Jacquet, S., Monnin, C., Herlory, O., Mille, D., Dufour, A., Oursel, B., Heimbürger-Boavida,
1125 L.E., D'onofrio, S., Layglon, N., Garnier, C., 2021. Characterization of the submarine
1126 disposal of a Bayer effluent (Gardanne alumina plant, southern France): I. Size
1127 distribution, chemical composition and settling rate of particles forming at the outfall.
1128 Chemosphere, 263, 127695. doi: https://doi.org/10.1016/j.chemosphere.2020.127695.
1129 Jiskra, M., Heimbürger-Boavida, L.E., Desgranges, M.M., Petrova M.V., Dufour, A.,
1130 Ferreira-Araujo, B., Masbou, J., Chmeleff, J., Thyssen, M., Point, D., Sonke, J.E., 2021.
1131 Mercury stable isotopes constrain atmospheric sources to the ocean. Nature, 597, 678–682.
1132 doi: 10.1038/s41586-021-03859-8
1133 Jordi, A., Basterretxea, G., Tovar-Sanchez, A., Alastuey, A., Querol, X., 2012. Copper
1134 aerosols inhibit phytoplankton growth in the Mediterranean Sea. Proceedings of the
1135 National Academy of Sciences, 109, 21246–21249. doi: 10.1073/pnas.1207567110.
1136 Köck-Schulmeyer, M., Ginebreda, A., Petrovic, M., Giulivo, M., Aznar-Alemany, Ò.,
1137 Eljarrat, E., Valle-Sistac, J., Molins-Delgado, D., Diaz-Cruz, M.S., Monllor-Alcaraz, L.S.,
1138 Guillem-Argiles, N., Martínez, E., Miren, L.A., Llorca, M., Farré, M., Peña, J.M.,

1139 Mandaric, L., Pérez, S., Majone, B., Bellin, A., Kalogianni, E., Skoulikidis, N.T., Milačič,
1140 R., Barceló, D., 2021. Priority and emerging organic microcontaminants in three
1141 Mediterranean river basins: Occurrence, spatial distribution, and identification of river
1142 basin specific pollutants. Science of the Total Environment, 754, 142344. doi:
1143 10.1016/j.scitotenv.2020.142344
1144 Lascaratos, A., Williams, R.G., Tragou, E., 1993. A mixed-layer study of the formation of
1145 Levantine Intermediate Water. Journal of Geophysical Research: Oceans, 98 (C8), 14739–
1146 14749.
1147 Leblanc, K., Quéguiner, B., Diaz, F., Cornet, V., Michel-Rodriguez, M., Durrieu de Madron,
1148 X., Bowler, C., Malviya, S., Thyssen, M., Gregori, G., Rembauville, M., Grosso, O.,
1149 Poulain, J., de Vargas, C., Pujo-Pay, M., Conan, P., 2018. Nanoplanktonic diatoms are
1150 globally overlooked but play a role in spring blooms and carbon export. Nature
1151 Communication, 9, 953. doi: 10.1038/s41467-018-03376-9
1152 Lee, C.S., Fisher, N.S., 2016. Methylmercury uptake by diverse marine phytoplankton.
1153 Limnology and Oceanography, 61, 1626–1639. doi: 10.1002/lno.10318
1154 Lejeusne, C., Chevaldonné, P., Pergent-Martini, C., Boudouresque, C.F., Pérez, T., 2010.
1155 Climate change effects on a miniature ocean: the highly diverse, highly impacted
1156 Mediterranean Sea. Trends in Ecology and Evolution, 25, 250–260. doi:
1157 10.1016/j.tree.2009.10.009
1158 Li, H., Duan, D., Beckingham, B., Yang, Y., Ran, Y., Grathwohl, P., 2020. Impact of trophic
1159 levels on partitioning and bioaccumulation of polycyclic aromatic hydrocarbons in
1160 particulate organic matter and plankton. Marine Pollution Bulletin, 160, 111527. doi:
1161 10.1016/j.marpolbul.2020.111527
1162 Li, Z., Chi, J., Wu, Z., Zhang, Y., Liu, Y., Huang, L., Lu, Y., Uddin, M., Zhang, W., Wand,
1163 X., Lin, Y., Tong, Y., 2021. Characteristics of plankton Hg bioaccumulations based on a

1164 global data set and the implications for aquatic systems with aggravating nutrient
1165 imbalance. Frontiers of Environmental Science & Engineering, 16, 37. doi:
1166 10.1007/s11783-021-1471-x
1167 Lipiatou, E., Albaigés, J., 1994. Atmospheric deposition of hydrophobic organic chemicals in
1168 the northwestern Mediterranean Sea: comparison with the Rhone river input. Marine
1169 Chemistry, 46, 153–164. doi: 10.1016/0304-4203(94)90052-3
1170 Llamas-Dios, M.I., Vadillo, I., Jimenez-Gavilan, P., Candela, L., Corada-Fernandez, C., 2021.
1171 Assessment of a wide array of contaminants of emerging concern in a Mediterranean water
1172 basin (Guadalhorce river, Spain): Motivations for an improvement of water management
1173 and pollutants surveillance. Science of the Total Environment, 788, 147822. doi:
1174 0.1016/j.scitotenv.2021.147822
1175 Marañón, E., Wambeke, F., Uitz, J., Boss, E., Dimier, C., Dinasquet, J., Engel, A., Haëntjens,
1176 N., Pérez-Lorenzo, M., Taillandier, V., Zäncker, B., 2021. Deep maxima of phytoplankton
1177 biomass, primary production and bacterial production in the Mediterranean Sea.
1178 Biogeosciences, 18, 1749–1767. doi: 10.5194/bg-18-1749-2021
1179 Margirier, F., Testor, P., Heslop, E., Mallil, K., Bosse, A., Houpert, L., Mortier, L., Bouin,
1180 M.-N., Coppola, L., D'Ortenzio, F., Durrieu de Madron, X., Mourre, B., Prieur, L.,
1181 Raimbault, P., Taillandier, V., 2020. Abrupt warming and salinification of intermediate
1182 waters interplays with decline of deep convection in the Northwestern Mediterranean Sea.
1183 Scientific Reports, 10, 20923. doi: 10.1038/s41598-020-77859-5
1184 Martin, J.H., Knauer, G.A., 1973. The elemental composition of plankton. Geochimica
1185 Cosmochimica Acta, 37, 1639–1653. doi: 10.1016/0016-7037(73)90154-3
1186 Mayot, N., D'Ortenzio, F., Uitz, J., Gentili, B., Ras, J., Vellucci, V., Golbol, M., Antoine, D.,
1187 Claustre, H., 2017. Influence of the Phytoplankton Community Structure on the Spring and

1188 Annual Primary Production in the Northwestern Mediterranean Sea, Journal of
1189 Geophysical Research Oceans, 122, 9918–9936. doi:10.1002/2016JC012668
1190 Millot, C., 1999. Circulation in the Western Mediterranean Sea. Journal of Marine Systems,
1191 20, 423–442. doi: 10.1016/S0924-7963(98)00078-5
1192 Millot, C., Taupier-Letage, I., 2005. Circulation in the Mediterranean Sea. The Handbook of
1193 Environmental Chemistry, vol. K 29–66. doi: 10.1007/b107143
1194 Morales, L., Dachs, J., Fernández-Pinos, M.C., Berrojalbiz, N., Mompean, C., González-
1195 Gaya, B., Jiménez, B., Bode, A., Abalos, M., Abad, E., 2015. Oceanic sink and
1196 biogeochemical controls on the accumulation of polychlorinated dibenzo-pdioxins,
1197 dibenzofurans, and biphenyls in plankton. Environmental Science and Technology, 49,
1198 13853–13861. doi: 10.1021/acs.est.5b01360
1199 Nizzetto, L., Gioia, R., Li, J., Borga, K., Pomati, F., Bettinetti, R., Dachs, J., Jones, K.C.,
1200 2012. Biological pump control of the fate and distribution of hydrophobic organic
1201 pollutants in water and plankton. Environmental Science and Technology, 46, 3204–3211.
1202 doi: 10.1021/es204176q
1203 Oursel, B., Garnier, C., Durrieu, G., Mounier, S., Omanović, D., Lucas, Y., 2013. Dynamics
1204 and fates of trace metals chronically input in a Mediterranean coastal zone impacted by a
1205 large urban area. Marine Pollution Bulletin, 69, 137–149. doi:
1206 10.1016/j.marpolbul.2013.01.023
1207 Radakovitch, O., Roussiez, V., Ollivier, P., Ludwig, W., Grenz, C., Probst, J.L., 2008.
1208 Particulate heavy metals input from rivers and associated sedimentary deposits on the Gulf
1209 of Lion continental shelf. Estuarine, Coastal and Shelf Science, 77, 285–295. doi:
1210 10.1016/j.ecss.2007.09.028
1211 Ramírez-Romero, E., Molinero, J.C., Sommer, U., Salhi, N., Kefi- Daly Yahia, O., Daly
1212 Yahia, M.N., 2020. Phytoplankton size changes and diversity loss in the southwestern

1213 Mediterranean Sea in relation to long-term hydrographic variability. Estuarine, Coastal and
1214 Shelf Science, 235, 106574. doi: 10.1016/j.ecss.2019.106574
1215 Reygondeau, G., Guieu, C., Benedetti, F., Irisson, J.O., Ayata, S.D., Gasparini, S., Koubbi, P.,
1216 2017. Biogeochemical regions of the Mediterranean Sea: an objective multidimensional
1217 and multivariate environmental approach. Progress in Oceanography, 151, 138–148. doi:
1218 10.1016/j.pocean.2016.11.001
1219 Reygondeau, G., Irisson, J.-O., Ayata, S., Gasparini, S., Benedetti, F., Albouy, C., Hattab, T.,
1220 Guieu, C., Koubbi, P., 2014. Definition of the Mediterranean Eco-Regions and Maps of
1221 Potential Pressures in These Eco-Regions. Technical Report. Deliverable Nr. 1.6. FP7-
1222 PERSEUS project.
1223 Salat, J., Font, J., 1987. Water mass structure near and off shore the Catalan coast during the
1224 winters of 1982 and 1983. Annales Geophysicae, 1B, 49–54.
1225 Salgado-Hernanz, P.M., Racault, M.-F., Font-Muñoz, J.S., Basterretxea, G., 2019. Trends in
1226 phytoplankton phenology in the Mediterranean Sea based on ocean-colour remote sensing.
1227 Remote Sensing of Environment, 221, 50–64. doi: 10.1016/j.rse.2018.10.036
1228 Salhi, N., Zmerli Triki, H., Molinero, J.C., Laabir, M., Sehli, E., Bellaaj-Zouari, A., Daly
1229 Yahia, N., Kefi-Daly Yahia, O., 2018. Seasonal variability of picophytoplankton under
1230 contrasting environments in northern Tunisian coasts, southwestern Mediterranean Sea.
1231 Marine Pollution Bulletin, 129, 866–874. doi: 10.1016/j.marpolbul.2017.10.029
1232 Schlitzer, R., 2014. Ocean Data View. Available online at: http://odv.awi.de
1233 Ser-Giacomi, E., Jordá-Sánchez, G., Sotto-Navarro, J., Thomsen, S., Mignot, J., Sevault, F.,
1234 Rossi, V., 2020. Impact of climate change on surface stirring and transport in the
1235 Mediterranean Sea. Geophysical Research Letters, 47, e2020GL089941. doi:
1236 10.1029/2020GL089941

1237 Sicre, M.-A., Fernandes, M.B., Pont, D., 2008. Poly-aromatic hydrocarbon (PAH) inputs from
1238 the Rhône River to the Mediterranean Sea in relation with the hydrological cycle: Impact
1239 of floods. Marine Pollution Bulletin, 56, 1935–1942. doi: 10.1016/j.marpolbul.2008.07.015
1240 Siokou-Frangou, I., Christaki, U., Mazzocchi, M.G., Montresor, M., Ribera D'Alcala, M.,
1241 Vaque, D., Zingone, A., 2010. Plankton in the open mediterranean Sea: A review.
1242 Biogeosciences, 7, 1543–1586. doi: 10.5194/bg-7-1543-2010
1243 Strady, E., Harmelin-Vivien, M., Chiffoleau, J.F., Veron, A., Tronczynski, J., Radakovitch,
1244 O., 2015. ^{210}Po and ^{210}Pb trophic transfer within the phytoplankton–zooplankton–
1245 anchovy/sardine food web: a case study from the Gulf of Lion (NW Mediterranean Sea.
1246 Journal of Environmental Radioactivity, 143, 141–151. doi: 10.1016/j.jenvrad.2015.02.019
1247 Swackhamer, D.L., Skoglund, R.S., 1993. Bioaccumulation of PCBs by algae: kinetics versus
1248 equilibrium. Environmental Toxicology and Chemistry, 12, 831–838. doi:
1249 10.1002/etc.5620120506
1250 Tang, J., Wang, S., Tai, Y., Tam, N.F., Su, L., Shi, Y., Luo, B., Tao, R., Yang, Y., Zhang, X.,
1251 2020. Evaluation of factors influencing annual occurrence, bioaccumulation, and
1252 biomagnification of antibiotics in planktonic food webs of a large subtropical river in
1253 South China. Water Research, 170, 115302. doi: 10.1016/j.watres.2019.115302
1254 Tao, Y., Xue, B., Lei, G., Liu, F., Wang, Z., 2017a. Effects of climate change on
1255 bioaccumulation and biomagnification of polycyclic aromatic hydrocarbons in the
1256 planktonic food web of a subtropical shallow eutrophic lake in China. Environmental
1257 Pollution, 223, 624–634. doi: 10.1016/j.envpol.2017.01.068
1258 Tao, Y., Yu, J., Liu, X., Xue, B., Wang, S., 2018. Factors affecting annual occurrence,
1259 bioaccumulation, and biomagnification of polycyclic aromatic hydrocarbons in plankton
1260 food webs of subtropical eutrophic lakes. Water Research, 132, 1–11. doi:
1261 10.1016/j.watres.2017.12.053

1262 Tao, Y., Yu, J., Xue, B., Yao, S., Wang, S., 2017b. Precipitation and temperature drive
1263 seasonal variation in bioaccumulation of polycyclic aromatic hydrocarbons in the
1264 planktonic food webs of a subtropical shallow eutrophic lake in China. Science of the Total
1265 Environment, 583, 447–457. doi: 10.1016/j.scitotenv.2017.01.100
1266 Tedetti, M., Guigue, C., Goutx, M., 2010. Utilization of a submersible UV fluorometer for
1267 monitoring anthropogenic inputs in the Mediterranean coastal waters. Marine Pollution
1268 Bulletin, 60, 350–362. doi: 10.1016/j.marpolbul.2009.10.018
1269 Tedetti, M., Tronczynski, J., 2019. HIPPOCAMPE cruise, RV Antea.
1270 https://doi.org/10.17600/18000900
1271 Tesán-Onrubia, J.A., Tedetti, M., Carlotti, F., Tenaille, M., Guilloux, L., Pagano, M.,
1272 Lebreton, B., Guillou, G., Fierro-González, P., Guigue, C., Chifflet, S., Garcia, T.,
1273 Boudriga, I., Belhassen, M., Bellaaj-Zouari, M., Bănaru, D., 2023. Spatial variations of
1274 stable isotope compositions and biochemical content of size-fractionated plankton in the
1275 Mediterranean Sea (MERITE-HIPPOCAMPE campaign). In revision to this special issue.
1276 The MerMex Group, 2011. Marine ecosystems' responses to climatic and anthropogenic
1277 forcings in the Mediterranean. Progress in Oceanography, 91, 97–166. doi:
1278 10.1016/j.pocean.2011.02.003
1279 Thieuleux, F., Moulin, C., Bréon, F.M., Maignan, F., Poitou, J., Tanré, D., 2005. Remote
1280 sensing of aerosols over the oceans using MSG/SEVIRI imagery. Annals of Geophysics,
1281 23, 3561–3568. doi: 10.5194/angeo-23-3561-2005
1282 Thomas, D.M., Lee, C.-S., Fisher, N.S., 2018. Bioaccumulation and trophic transfer of ^{137}Cs
1283 in marine and freshwater plankton. Chemosphere, 209, 599–607. doi:
1284 10.1016/j.chemosphere.2018.06.124
1285 Tiano, M., Tronczyński, J., Harmelin-Vivien, M., Tixier, C., Carlotti, F., 2014. PCB
1286 concentrations in plankton size classes, a temporal study in Marseille Bay, Western

Mediterranean Sea. Marine Pollution Bulletin, 89, 331–339. doi: 10.1016/j.marpolbul.2014.09.040

Tornero, V., Hanke, G., 2016. Chemical contaminants entering the marine environment from sea-based sources: A review with a focus on European seas. Marine Pollution Bulletin, 112, 17–38. doi: https://doi.org/10.1016/j.marpolbul.2016.06.091

Uitz, J., Claustre, H., Morel, A., Hooker, S.B., 2006. Vertical distribution of phytoplankton communities in open ocean: An assessment based on surface chlorophyll. Journal of Geophysical Research Oceans, 111, C08005. doi:10.1029/2005JC003207

UNEP/MAP, 2012. State of the Mediterranean Marine and Coastal Environment, UNEP/MAP – Barcelona Convention, Athens.

Vargaz-Yanez, M., Mallard, E.R.M., Zunino, P., Garcia-Martinez, M., Moya, F., 2012. The effect of interpolation methods in temperature and salinity trends in the western Mediterranean. Mediterranean Marine Science, 13, 118–125. doi: 10.12681/mms.28

Volpe, G., Colella, S., Brando, V.E., Forneris, V., La Padula, F., Di Cicco, A., Sammartino, M., Bracaglia, M., Artuso, F., Santoleri, R., 2019. Mediterranean ocean colour Level 3 operational multi-sensor processing. Ocean Science, 15, 127–146. doi: 10.5194/os-15-127-2019

Zouch, H., Cabrol, L., Chifflet, S., Tedetti, M., Karray, F., Zaghden, H., Sayadi, S., Quéméneur, M., 2018. Effect of acidic industrial effluent release on microbial diversity and trace metal dynamics during resuspension of coastal sediment. Frontiers in Microbiology, 9, 3103, doi: 10.3389/fmicb. 2018.03103

Figure captions

Figure 1. Conceptual scheme and questions addressed by the MERITE-HIPPOCAMPE cruise to identify the role of Mediterranean plankton as biological pump of contaminants. It considers the accumulation and transfer of metallic/metalloid/organometallic and organic contaminants at the atmosphere-water-plankton interfaces and through the planktonic food webs, i.e., phyto-, zoo- and bacterio-plankton, with the deep chlorophyll maximum (DCM) as privileged study zone.

Figure 2. a) Location of the ten stations (black circles) investigated during the MERITE-HIPPOCAMPE cruise (13 April–14 May 2019) along a North-South transect in the Mediterranean Sea on board the R/V *Antea*. The main characteristics of these stations are provided in Table 1. In addition, two other stations (T2 and T4, brown circles) were sampled in the Tunisian waters during leg 2 (2–3 May 2019) on board the R/V *Hannibal* for trawling of small pelagic fishes (see Table 2 for more details). Two ground stations, located in the northern part (Marseille, France) and southern part (Sfax, Tunisia) of the Mediterranean basin, were set up for the collection of atmospheric deposition samples from March 2019 to June 2020 (i.e., before, during and after the cruise). b) Cruise track with the position of the ten stations studied on board the R/V *Antea*. During leg 1 (13–28 April; from La Seyne-sur-Mer to Tunis), five stations were sampled: St2, St4, St3, S10 and St11 (in this chronological order), while the five other stations were sampled during leg 2 (30 April–14 May; from Tunis to Gulf of Gabès, and then return to La Seyne-sur-Mer): St15, St17, St19, St9 and St1 (in this chronological order).

Figure 3. Summary of our approach with 1) the collection of large amounts of plankton, suspended particles, and water in the deep chlorophyll maximum (DCM) and surface/subsurface waters (0–5 m depth) with various collecting instruments, 2) the separation of these materials into diverse size fractions by sieving or filtration, and the sharing of the obtained size fractions for numerous biological and chemical analyses. Adapted from Alcaraz and Calbet (2003).

Figure 4. Saharan dust event of April. Here is presented for 22 April 2019 which is the day where the dust plume was the most intense: a) Daily Aerosol Optical Depth (AOD, unitless) product from MSG-SEVIRI, b) MODIS image from NASA worldview, and BSC-DREAM-Dust forecast of c) dry and d) wet deposition (in mg m^{-2}).

Figure 5. Saharan dust event of May. Here is presented for 3 May 2019 which is the day where the dust was located over ship's position: a) Daily Aerosol Optical Depth (AOD, unitless) product from MSG-SEVIRI, b) MODIS image from NASA worldview, and BSC-DREAM-Dust forecast of c) dry and d) wet deposition (in mg m^{-2}).

Figure 6. Distribution of subsurface **a)** temperature (°C) and **b)** salinity along the North-South Mediterranean transect recorded continuously from the flow-through pumped seawater at 2-m depth. Ocean Data View (ODV) software version 4.6.5. Schlitzer, R., http://odv.awi.de. 2014.

Figure 7. Vertical profiles of temperature (°C), salinity, TChl*a* concentration (µg L^{-1}) and dissolved O_2 concentration (µmole kg^{-1}) issued from the main carousel CTD deployments (Seabird SBE 911*plus*) at stations St1–St9. The dotted lines represent the depth of sampling in

the deep chlorophyll maximum (DCM) for Niskin/Go-Flo bottles. In box, the depth of the station. One or two profiles are displayed for each station. For each profile, only data acquired during the upcast are presented.

Figure 8. Vertical profiles of temperature (°C), salinity, TChl*a* concentration (µg L^{-1}) and dissolved O_2 concentration (µmole kg^{-1}) issued from the main carousel CTD deployments (Seabird SBE 911*plus*) at stations St10–St19. The dotted lines represent the depth of sampling in the deep chlorophyll maximum (DCM) for Niskin/Go-Flo bottles. In box, the depth of the station. One or two profiles are displayed for each station. For each profile, only data acquired during the upcast are presented.

Figure 9. Temperature-salinity diagram and identification of the main waters masses encountered during the MERITE-HIPPOCAMPE cruise (RAW: resident Atlantic Water; NAW: new Atlantic Water; LIW: Levantine Intermediate Water; WIW: Western Mediterranean Intermediate Water; GG: Gulf of Gabès water). The colour code refers to a) depth (in m) and b) stations (St1–St19). Twenty-one carousel CTD casts were used for this plot. Ocean Data View (ODV) software version 4.6.5. Schlitzer, R., http://odv.awi.de. 2014.

Figure 10. Composite image of average surface chlorophyll *a* (Chl*a*) concentration (in µg L^{-1}) over the period (13 April–14 May 2019) and area of the MERITE-HIPPOCAMPE cruise from Multi Satellite products (MODIS-AQUA, NOAA20-VIIRS, NPP-VIIRS and Sentinel3A-OLCI) (L4 product level, 1-km resolution; Volpe et al., 2019). This composite image corresponds to the average of the 32 daily images (from 13 April to 14 May 2019) for which Chl*a* concentration was averaged during the 8 h of measurements in the area. Product

name: OCEANCOLOUR_MED_CHL_L4_REP_OBSERVATIONS_009_078. Obtained from EU Copernicus Marine Service Information (CMEMS; https://marine.copernicus.eu/).

Figure 11. Distribution of various biogeochemical parameters recorded at the deep chlorophyll maximum (DCM) across the ten stations, from the most coastal stations in the North (St1, St4) to the southernmost stations (St17, St19): a) depth of the DCM (in m), concentrations in b) total chlorophyll *a* (TChl*a*, in µg L^{-1}), c) particulate organic carbon (POC, in µg L^{-1}), d) silicates [$Si(OH)_4$, in µM], e) nitrates (NO_3^-, in µM), f) phosphates (PO_4^{3-}, in µM), g) dissolved organic carbon (DOC, in µM), and h) absorption of chromophoric dissolved organic matter at 254 nm (a_{CDOM}, in m^{-1}). Nutrients, DOC and a_{CDOM} were measured on the fraction < 0.7 µm, while TChl*a* and POC were measured on the fraction > 0.7 µm from samples collected with Niskin X bottles.

Figure 12. Principal component analysis (PCA), based on the Pearson's correlation matrix, applied on the main biogeochemical parameters recorded at each stations (St1–19) in the deep chlorophyll maximum (DCM): concentrations in silicates [$Si(OH)_4$, in µM], nitrates (NO_3^-, in µM), phosphates (PO_4^{3-}, in µM), total chlorophyll *a* (TChl*a*, in µg L^{-1}), particulate organic carbon (POC, in µg L^{-1}), dissolved organic carbon (DOC, in µM) and absorption of chromophoric dissolved organic matter at 254 nm (a_{CDOM}, in m^{-1}). Projection of variables (i.e., main biogeochemical parameters, in red) and distribution of samples (i.e., stations, in blue) on the first factorial plane (PC1 *versus* PC2). Four groups of samples (stations) are highlighted from this PCA and confirmed by a hierarchical ascendant classification (dissimilarity measurement between clusters based on Ward's method): 1) St2, St3, St4, St10, 2) St1, St11, St15, St17, 3) St9, and 4) St19.

Figure 13. Overview of the types of articles that are a part of this special issue in the frame of the MERITE-HIPPOCAMPE cruise.

1412 **Table 1.** Main characteristics of the ten stations investigated in spring during the MERITE-HIPPOCAMPE cruise (13 April–14 May 2019) on
1413 board the R/V *Antea* along a North-South transect in the Mediterranean Sea. The stations are presented in chronological order in leg 1 then leg 2.
1414

Leg	Station	Latitude (N)	Longitude (E)	Location	Features	Area	Depth (m)	Start of operations (dd/mm in 2019)	End of operations (dd/mm in 2019)
1	St2	42° 56.020'	5° 58.041'	Offshore Toulon	Limit of the continental shelf; Boundary of the Ligurian consensus region[d]; Intermittently bloom area or bloom area (cluster #4 or #5)[e]	French	1770	14/04	16/04
	St4	43° 14.500'	5° 17.500'	Bay of Marseille (SOLEMIO[a] station)	Urbanised bay; Intermittently bloom area or bloom area (cluster #4 or #5)[e]	French	58	16/04	18/04
	St3	43° 08.150'	5° 15.280'	Offshore Marseille (JULIO[b] station)	Southeast entrance to the Gulf of Lion; Intrusions of the Ligurian-Provençal current; Intermittently bloom area or bloom area (cluster #4 or #5)[e]	French	95	18/04	20/04
	St10	40° 18.632'	7° 14.753'	Offshore (station 2 of PEACETIME cruise[c])	Slightly north of the North Balearic Front; Intermittently bloom area (cluster #4)[e]	Italian	2791	22/04	24/04
	St11	39° 07.998'	7° 41.010'	Offshore (station 3 of PEACETIME cruise[c])	South of the North Balearic Front; Algerian consensus region[d]; Presence of mesoscale eddies; No bloom area (cluster #3)[e]	Italian	1378	25/04	26/04

2	St15	36° 12.883'	11° 07.641'	Gulf of Hammamet	Close to the Sicily Channel; Possible entrance of Atlantic Tunisian Current branch; No bloom area (cluster #3)[e]; High density of small pelagic fishes	Tunisian	100	29/04	30/04
	St17	34° 30.113'	11° 43.573'	North of Gulf of Gabès	Gabès consensus region[d] boundary; Shallow area, influence of tides and Atlantic Tunisian Current; Coastal bloom area (cluster #6)[e]; High density of small pelagic fishes	Tunisian	50	01/05	02/05
	St19	33° 51.659'	11° 18.509'	South of Gulf of Gabès	Gabès consensus region[d]; Shallow area, influence of tides and Atlantic Tunisian Current; Coastal bloom area (cluster #6)[e]; High density of small pelagic fishes	Tunisian	50	02/05	05/05
	St9	41° 53.508'	6° 19.998'	Offshore (station 1 of PEACETIME cruise[c])	North of the North Balearic Front; Boundary of the Ligurian consensus region[d]; Winter convection area; Bloom area (cluster #5)[e]	French	2575	08/05	09/05
	St1	43° 03.819'	5° 59.080'	Bay of Toulon	Nearly closed urbanised bay; Intermittently bloom area or bloom area (cluster #4 or #5)[e]	French	91	10/05	11/05

[a] The SOLEMIO station *(Site d'Observation Littoral pour l'Environnement du MIO*) is part of the French national network of coastal observation SOMLIT (*Service d'Observation en Milieu LITtoral* – http://somlit.epoc.u-bordeaux1.fr/fr/).

[b] The JULIO station (*JUdicious Location for Intrusions Observations*) is dedicated to the study of the intrusions of the Ligurian-Provençal current.

[c] The PEACETIME cruise (*ProcEss studies at the Air-sEa Interface after dust deposition in the MEditerranean sea*) took place in May-June 2017 (http://peacetime-project.org/; Guieu et al., 2020).

[d] Consensus regions of the Mediterranean Sea as defined by Ayata et al. (2018).

[e] Bloom/cluster areas as defined by D'Ortenzio and d'Alcalà (2009) from SeaWiFS satellite surface TChl*a* concentration observations.

Table 2. Main characteristics of the two stations investigated during the MERITE-HIPPOCAMPE cruise in May 2019 on board the R/V *Hannibal* in the Tunisian waters for trawling of small pelagic fishes.

Station	Latitude (N)	Longitude (E)	Location	Depth (m)	Date (dd/mm in 2019)	Trawling duration
T2	34° 11.892'	10° 58.152'	Gulf of Gabès	45	02/05	0h40
T4	36° 59.142'	10° 19.734'	Gulf of Tunis	37	03/05	1h30

Table 3. Information about wet (rain) atmospheric deposition samples collected on board the R/V *Antea* during the MERITE-HIPPOCAMPE cruise.

Sample	**Station**	**Start date of sampling**	**Start time of sampling (UT)**	**End date of sampling (dd/mm in 2019)**	**End time of sampling (UT)**	**Type of deposition**
Rain 1	St10	22/04/19	19h15	23/04	9h45	Rain
Rain 2	St10	24/04/19	7h30	24/04	12h30	Rain
Rain 3	St11	26/04/19	3h15	26/04	12h00	Rain
Rain 4	St19	03/05/19	5h45	03/05	14h00	Rain
Rain 5	Transit from off Djerba to off Zarzis	03/05/19	16h45	04/05	9h00	Dry deposition + rain
Rain 6	St1	11/05/19	3h00	11/05	6h15	Rain

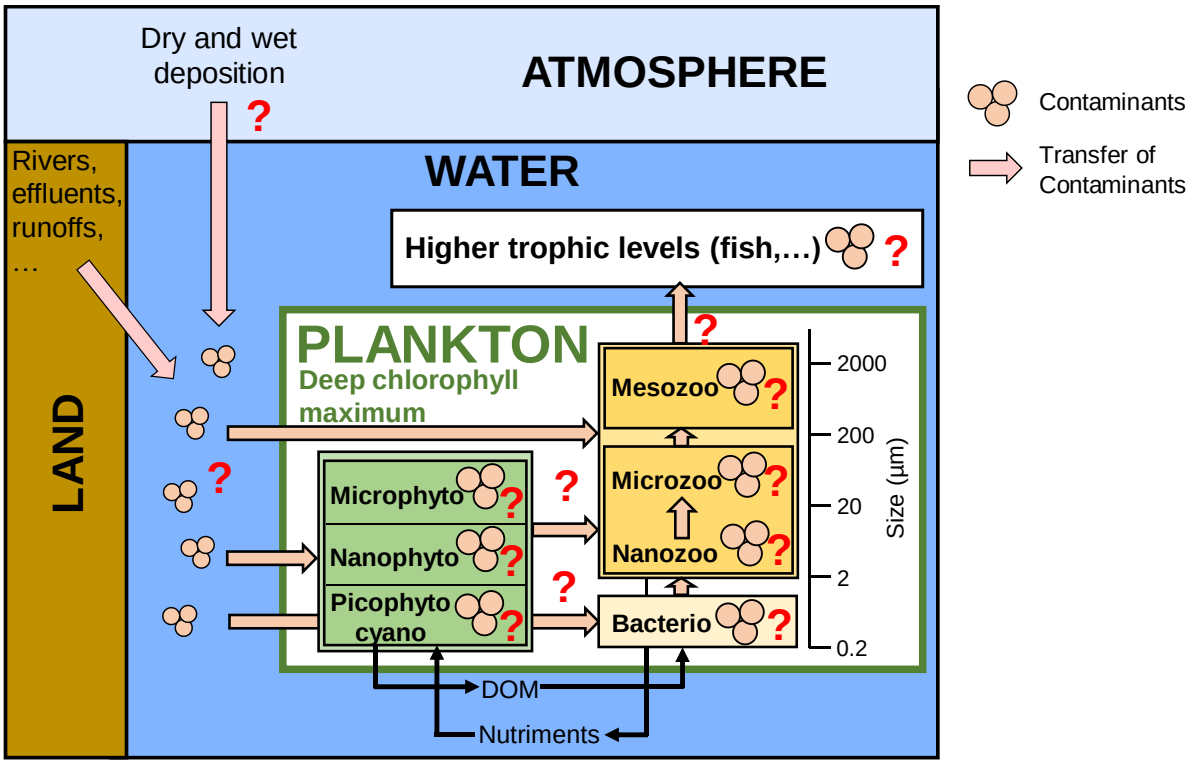
Dry and wet deposition
ATMOSPHERE
Rivers, effluents, runoffs, …
WATER
LAND
Higher trophic levels (fish,…)
PLANKTON
Deep chlorophyll maximum
Microphyto
Nanophyto
Picophyto cyano
Mesozoo
Microzoo
Nanozoo
Bacterio
2000
200
20
2
0.2
Size (µm)
DOM
Nutriments
Contaminants
Transfer of Contaminants

Figure 1

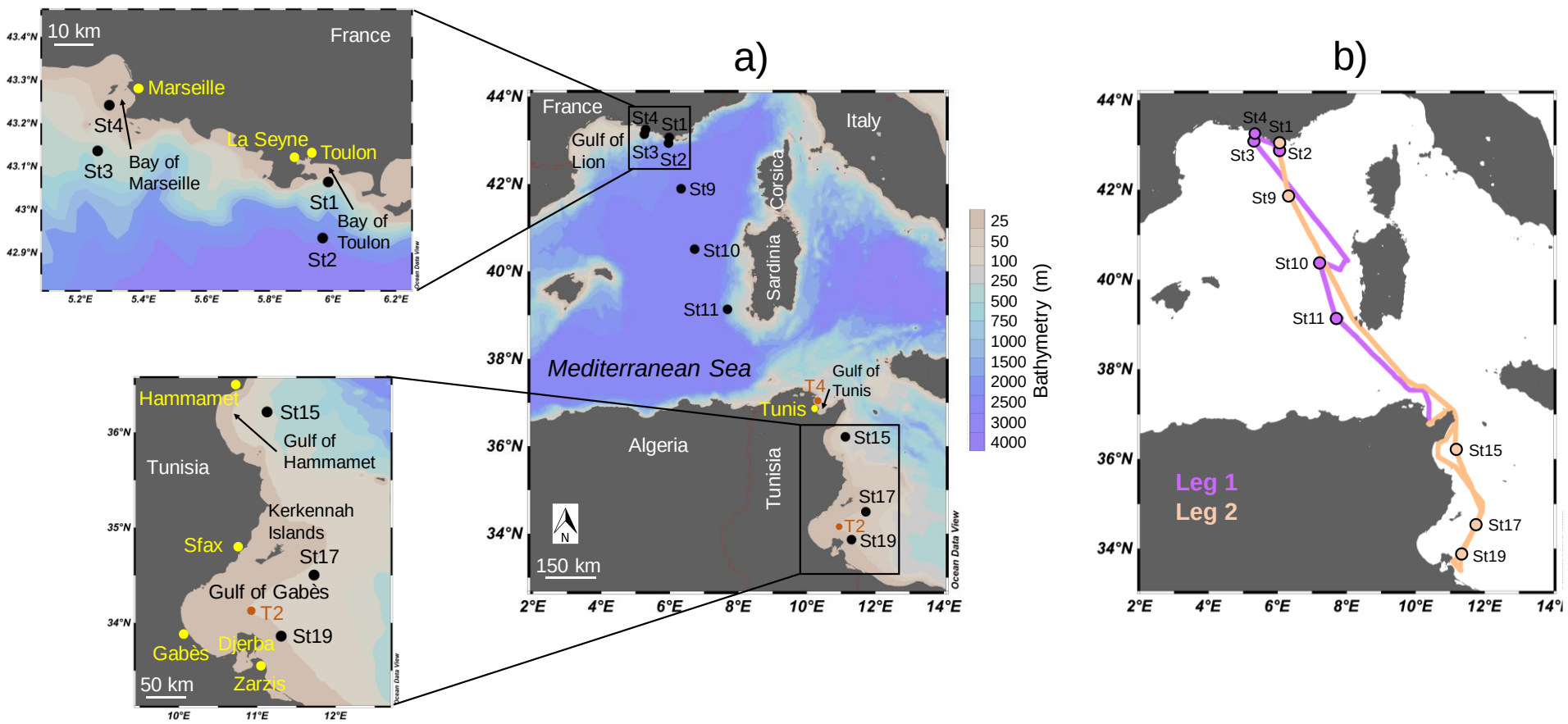
a)
b)
10 km
France
Marseille
St4
St3
Bay of
Marseille
La Seyne
Toulon
St1
Bay of
Toulon
St2
Hammamet
St15
Gulf of
Hammamet
Tunisia
Kerkennah
Islands
Sfax
St17
Gulf of Gabès
T2
St19
Gabès
Djerba
Zarzis
50 km
France
Gulf of
Lion
St4
St1
St3
St2
St9
Corsica
Italy
St10
Sardinia
St11
Mediterranean Sea
Gulf of
Tunis
T4
Tunis
Algeria
Tunisia
St15
St17
T2
St19
150 km
N
Bathymetry (m)
25
50
100
250
500
750
1000
1500
2000
2500
3000
4000
Leg 1
Leg 2

Figure 2

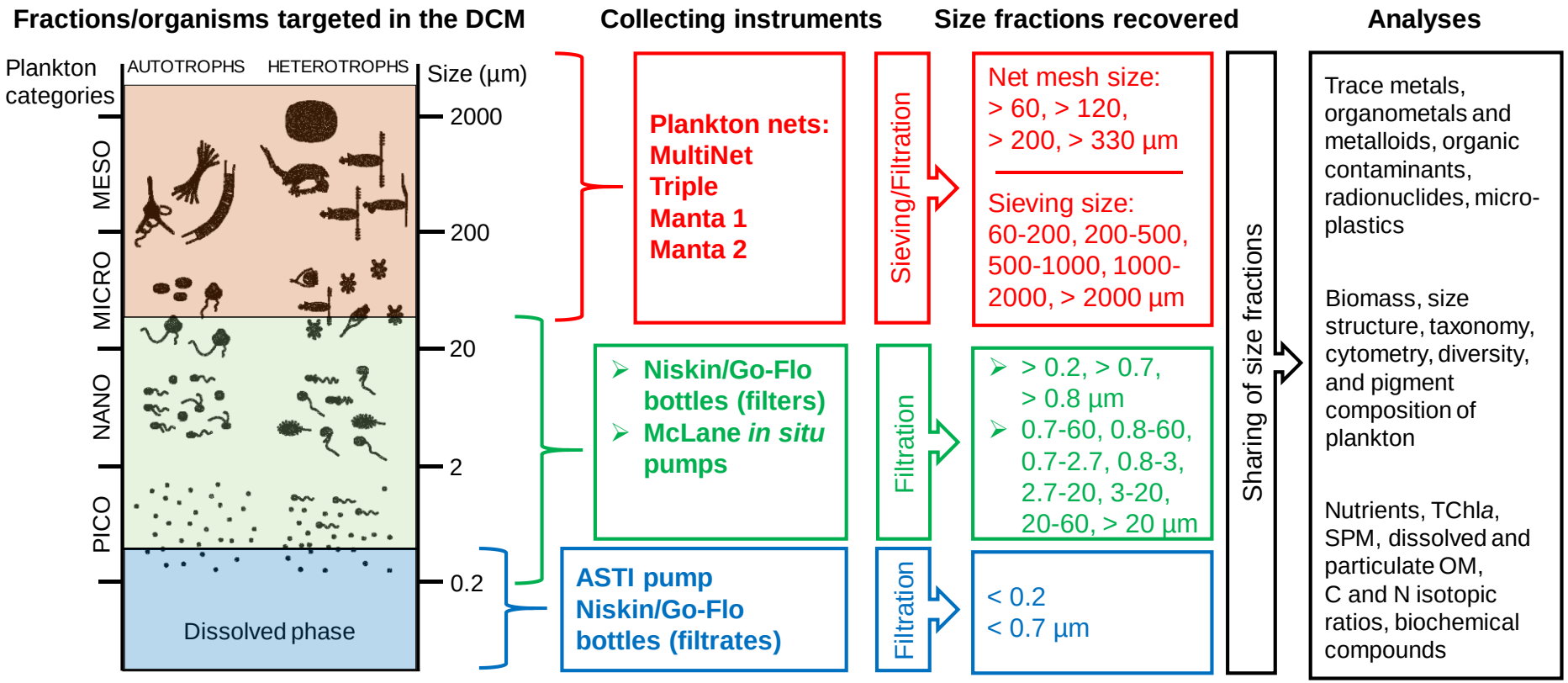
Fractions/organisms targeted in the DCM
Collecting instruments
Size fractions recovered
Analyses
Plankton categories
AUTOTROPHS
HETEROTROPHS
Size (µm)
MESO
MICRO
NANO
PICO
2000
200
20
2
0.2
Dissolved phase
Plankton nets:
MultiNet
Triple
Manta 1
Manta 2
Sieving/Filtration
Net mesh size:
> 60, > 120,
> 200, > 330 µm
Sieving size:
60-200, 200-500,
500-1000, 1000-
2000, > 2000 µm
Niskin/Go-Flo bottles (filters)
McLane in situ pumps
Filtration
> 0.2, > 0.7,
> 0.8 µm
0.7-60, 0.8-60,
0.7-2.7, 0.8-3,
2.7-20, 3-20,
20-60, > 20 µm
ASTI pump
Niskin/Go-Flo bottles (filtrates)
Filtration
< 0.2
< 0.7 µm
Sharing of size fractions
Trace metals, organometals and metalloids, organic contaminants, radionuclides, micro-plastics
Biomass, size structure, taxonomy, cytometry, diversity, and pigment composition of plankton
Nutrients, TChla, SPM, dissolved and particulate OM, C and N isotopic ratios, biochemical compounds

Figure 3

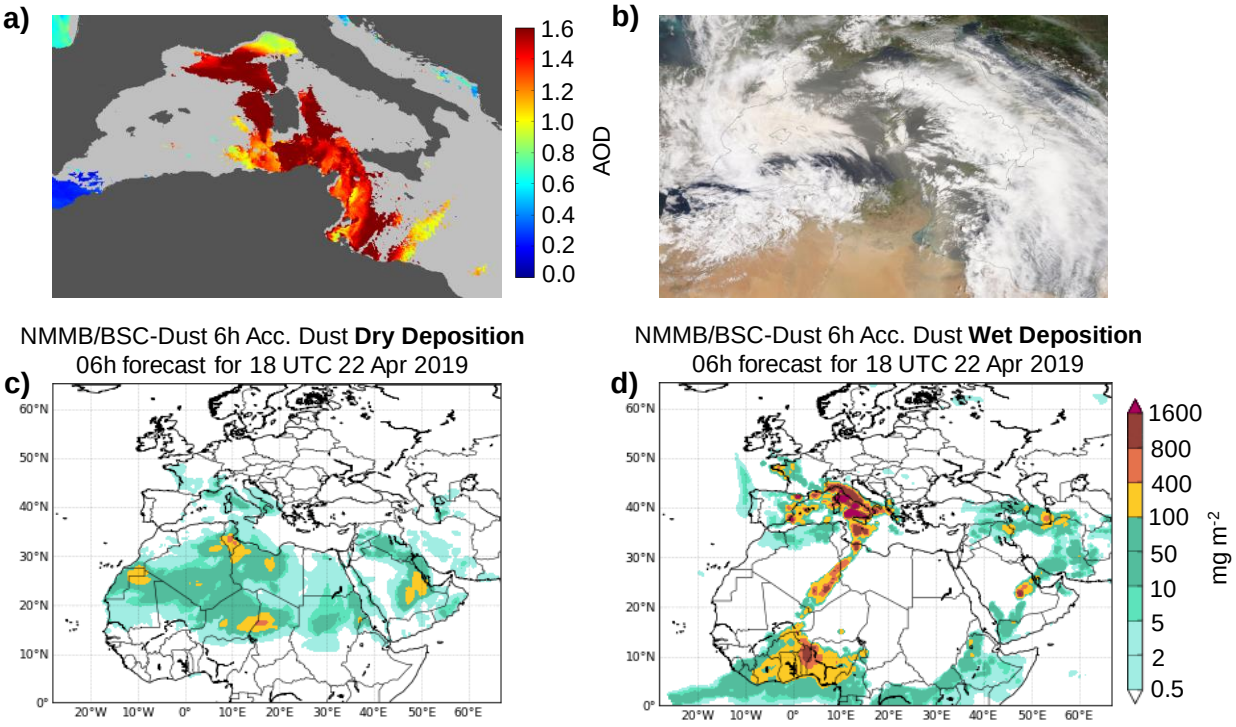
a)
1.6
1.4
1.2
1.0
0.8
0.6
0.4
0.2
0.0
AOD
b)
NMMB/BSC-Dust 6h Acc. Dust **Dry Deposition**
06h forecast for 18 UTC 22 Apr 2019
NMMB/BSC-Dust 6h Acc. Dust **Wet Deposition**
06h forecast for 18 UTC 22 Apr 2019
c)
d)
60°N
50°N
40°N
30°N
20°N
10°N
0°
20°W
10°W
0°
10°E
20°E
30°E
40°E
50°E
60°E
1600
800
400
100
50
10
5
2
0.5
mg m-2

Figure 4

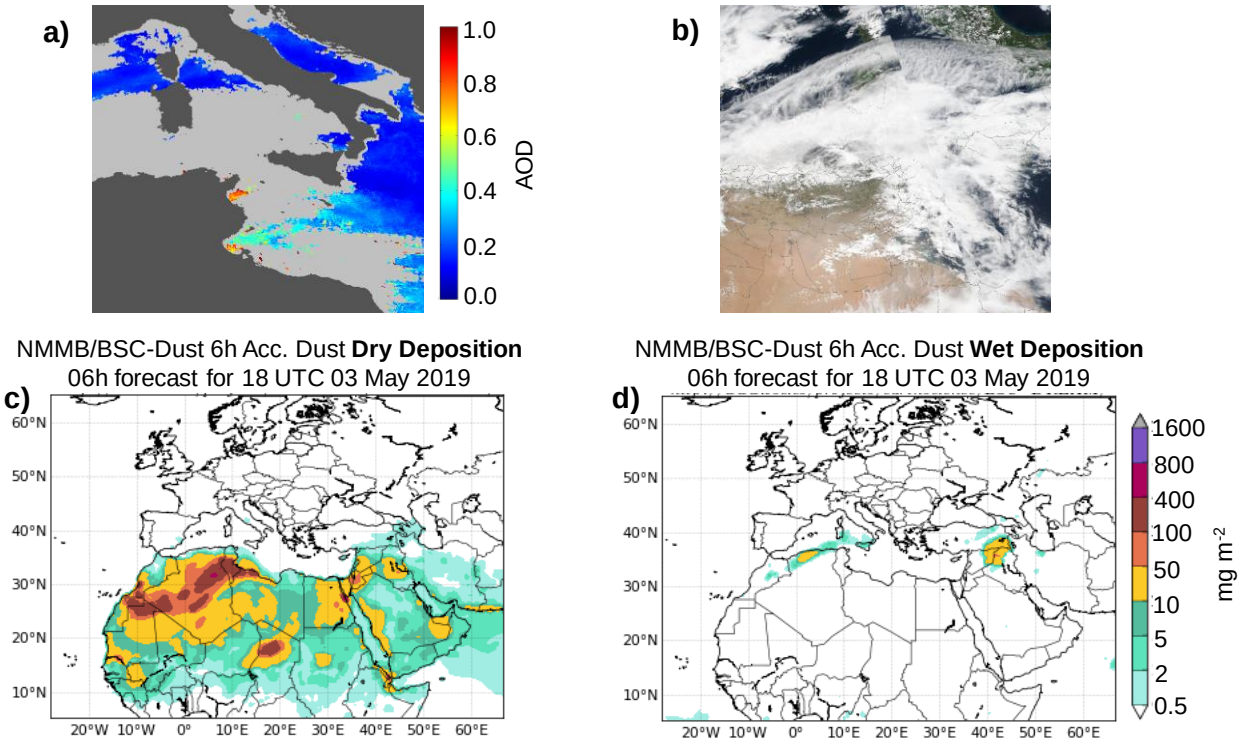
a)
1.0
0.8
0.6
0.4
0.2
0.0
AOD
b)
NMMB/BSC-Dust 6h Acc. Dust **Dry Deposition**
06h forecast for 18 UTC 03 May 2019
NMMB/BSC-Dust 6h Acc. Dust **Wet Deposition**
06h forecast for 18 UTC 03 May 2019
c)
d)
60°N
50°N
40°N
30°N
20°N
10°N
20°W 10°W 0° 10°E 20°E 30°E 40°E 50°E 60°E
1600
800
400
100
50
10
5
2
0.5
mg m-2

Figure 5

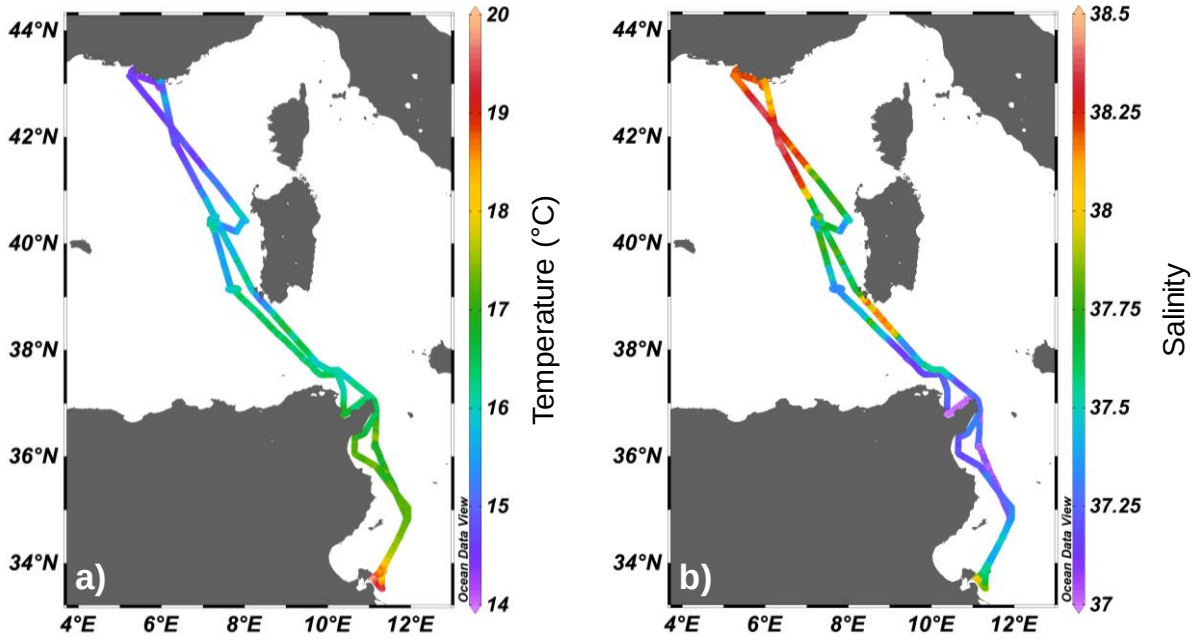
44°N
42°N
40°N
38°N
36°N
34°N
4°E
6°E
8°E
10°E
12°E
a)
b)
Ocean Data View
20
19
18
17
16
15
14
Temperature (°C)
38.5
38.25
38
37.75
37.5
37.25
37
Salinity

Figure 6

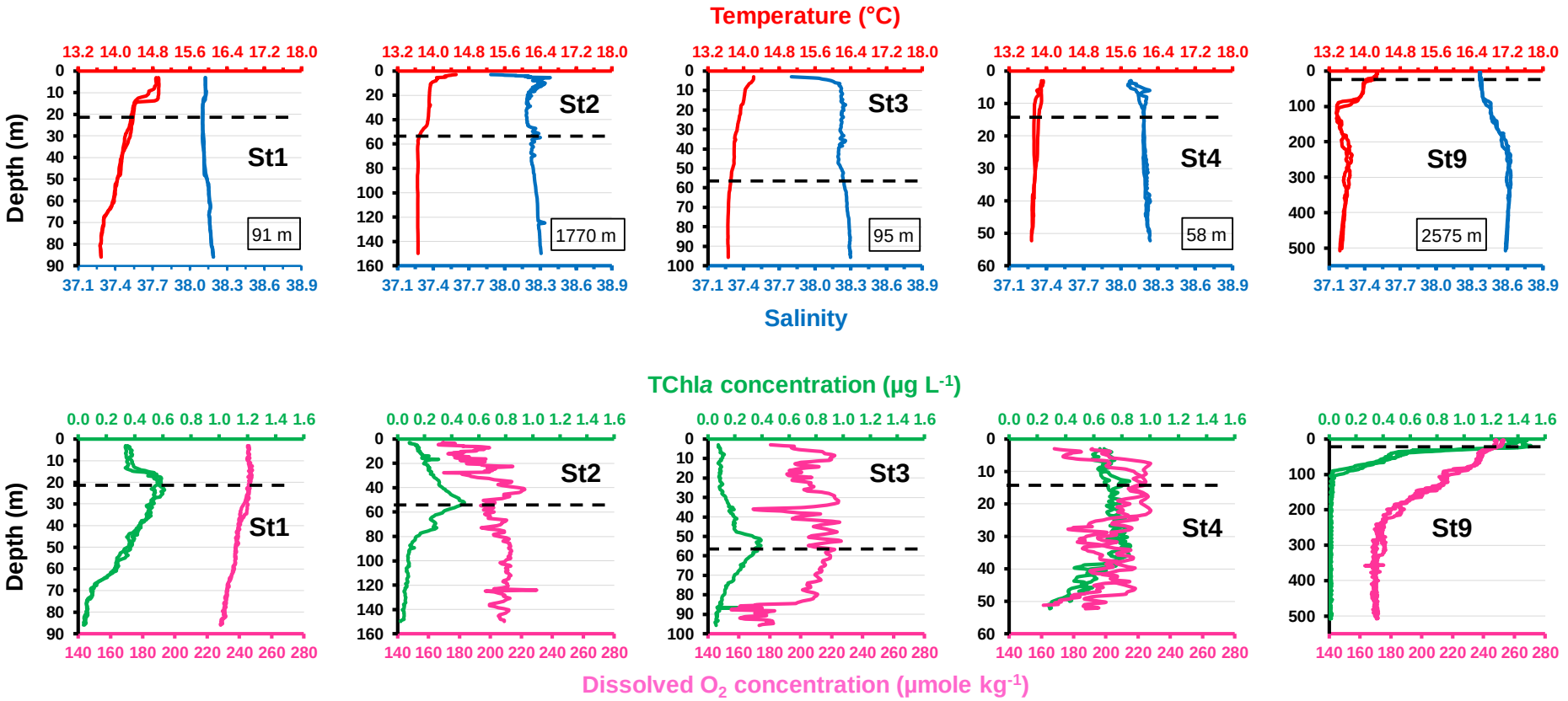
Temperature (°C)
13.2 14.0 14.8 15.6 16.4 17.2 18.0
Depth (m)
St1
91 m
St2
1770 m
St3
95 m
St4
58 m
St9
2575 m
37.1 37.4 37.7 38.0 38.3 38.6 38.9
Salinity
TChla concentration (µg L-1)
0.0 0.2 0.4 0.6 0.8 1.0 1.2 1.4 1.6
140 160 180 200 220 240 260 280
Dissolved O2 concentration (µmole kg-1)

Figure 7

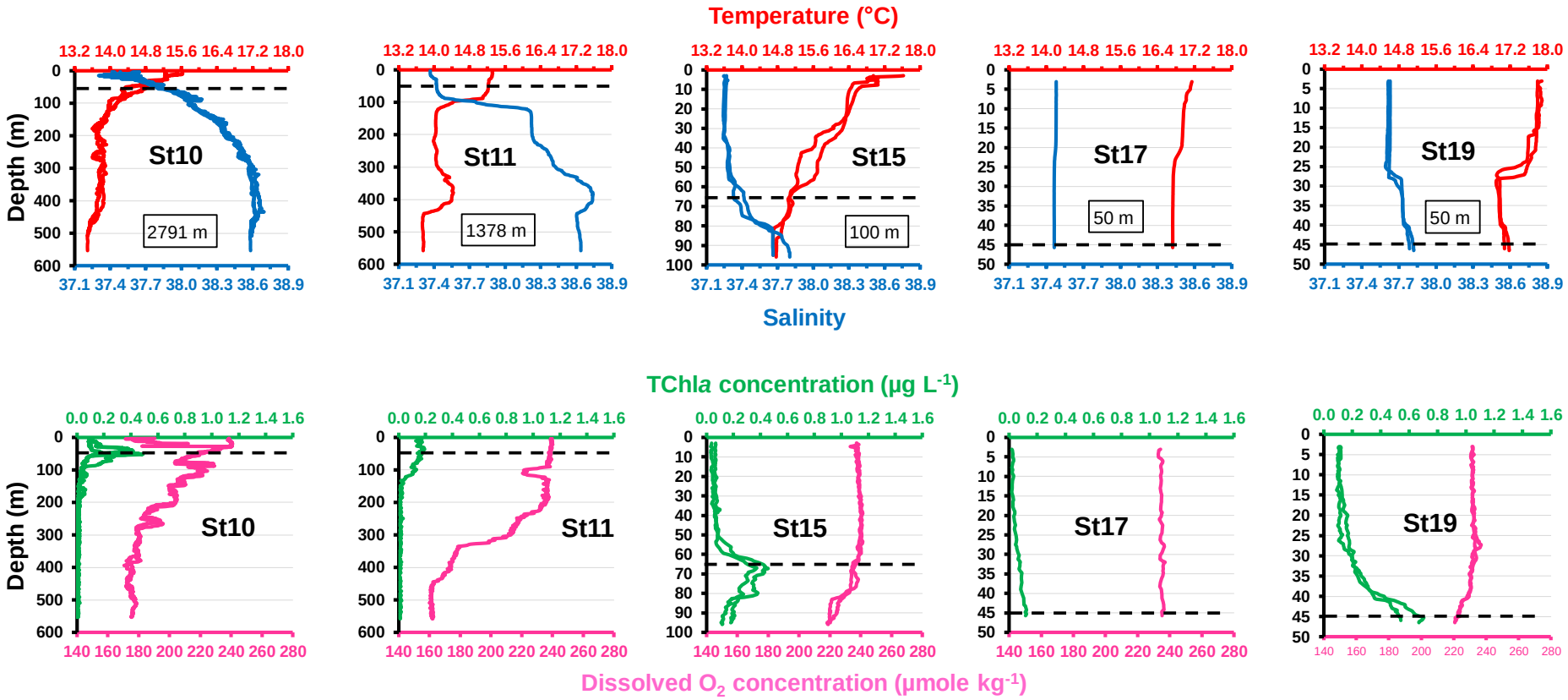
Temperature (°C)
13.2 14.0 14.8 15.6 16.4 17.2 18.0
Depth (m)
St10
2791 m
St11
1378 m
St15
100 m
St17
50 m
St19
50 m
37.1 37.4 37.7 38.0 38.3 38.6 38.9
Salinity
TChla concentration (µg L-1)
0.0 0.2 0.4 0.6 0.8 1.0 1.2 1.4 1.6
140 160 180 200 220 240 260 280
Dissolved O2 concentration (µmole kg-1)

Figure 8

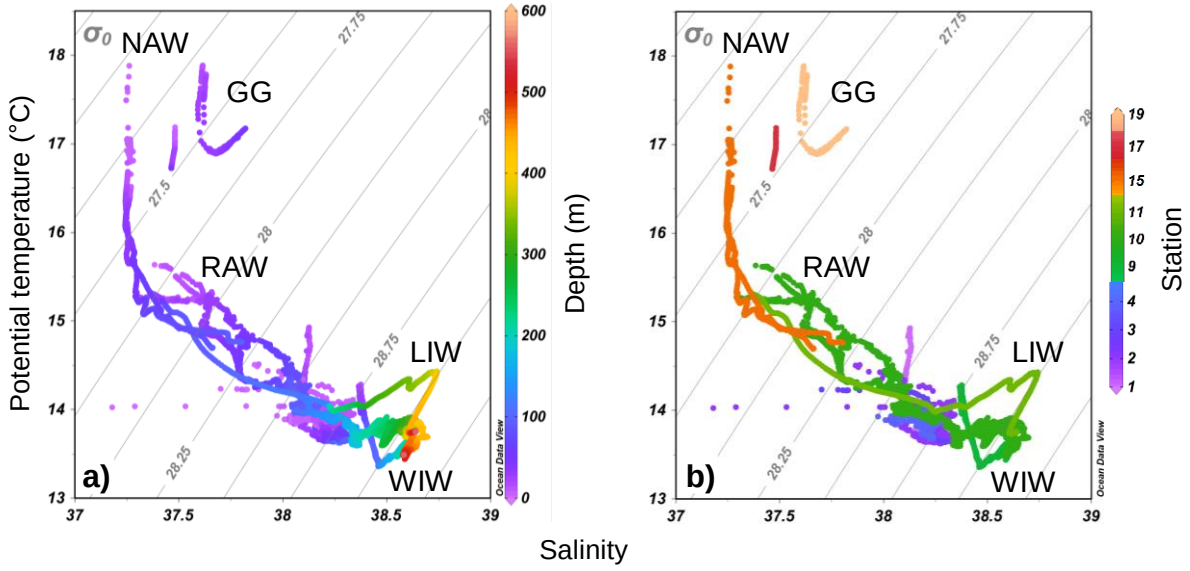
σ0
NAW
GG
RAW
LIW
WIW
a)
b)
Potential temperature (°C)
Salinity
Depth (m)
Station
Ocean Data View

Figure 9

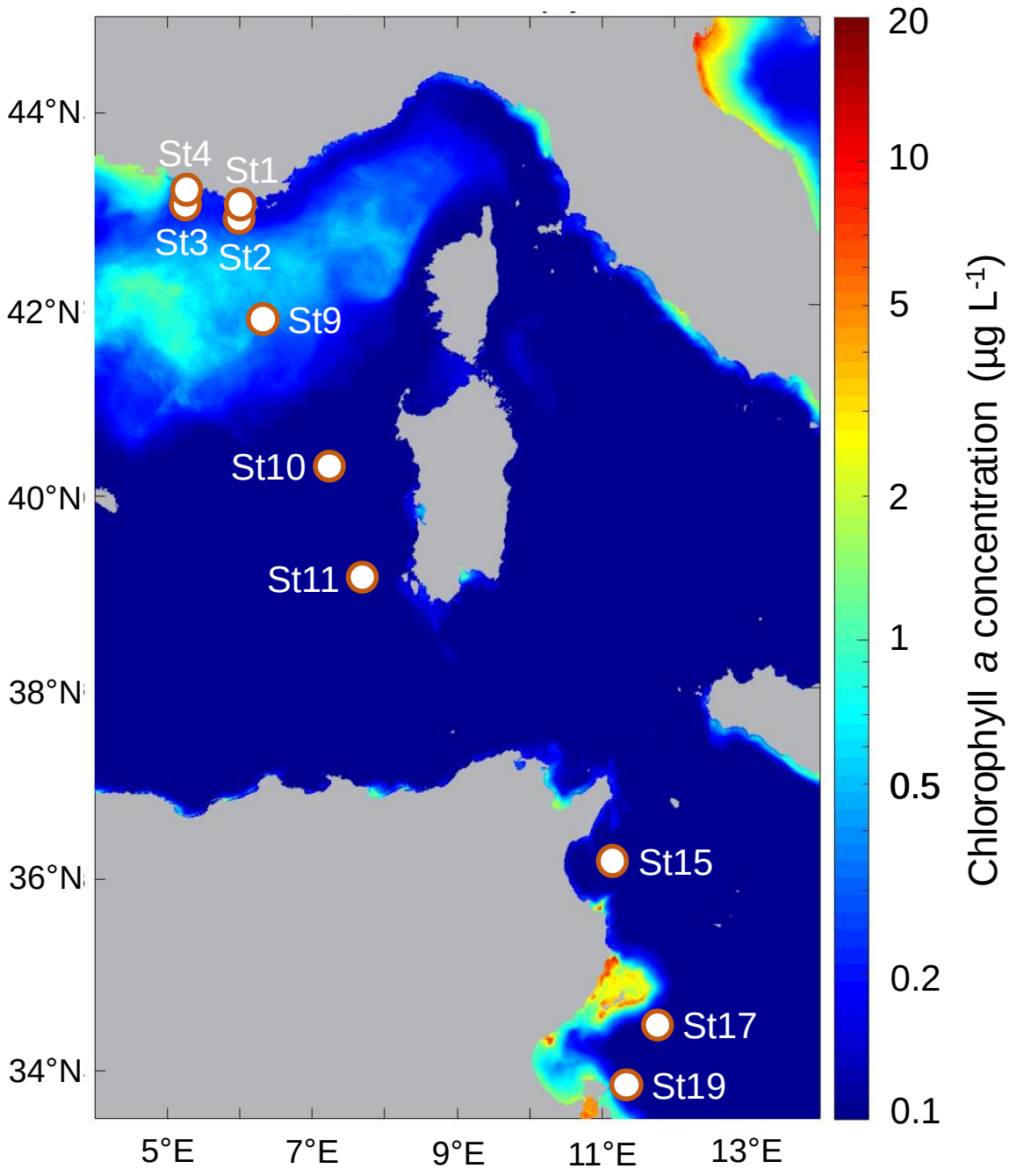
St4
St1
St3
St2
St9
St10
St11
St15
St17
St19
44°N
42°N
40°N
38°N
36°N
34°N
5°E
7°E
9°E
11°E
13°E
20
10
5
2
1
0.5
0.2
0.1
Chlorophyll a concentration (µg L-1)

Figure 10

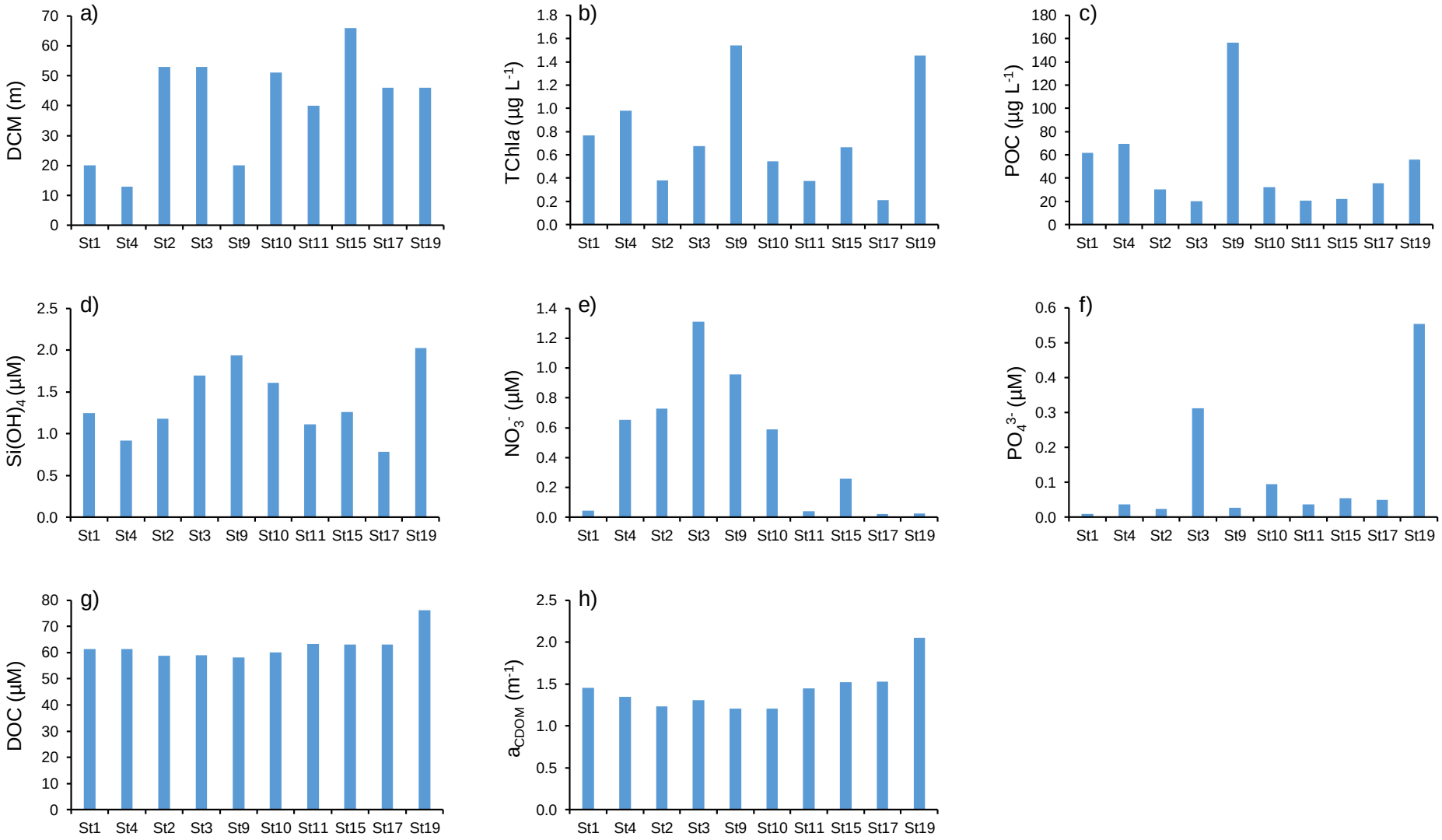
a)
DCM (m)
0
10
20
30
40
50
60
70
St1 St4 St2 St3 St9 St10 St11 St15 St17 St19
b)
TChla (µg L-1)
0.0
0.2
0.4
0.6
0.8
1.0
1.2
1.4
1.6
1.8
St1 St4 St2 St3 St9 St10 St11 St15 St17 St19
c)
POC (µg L-1)
0
20
40
60
80
100
120
140
160
180
St1 St4 St2 St3 St9 St10 St11 St15 St17 St19
d)
Si(OH)4 (µM)
0.0
0.5
1.0
1.5
2.0
2.5
St1 St4 St2 St3 St9 St10 St11 St15 St17 St19
e)
NO3- (µM)
0.0
0.2
0.4
0.6
0.8
1.0
1.2
1.4
St1 St4 St2 St3 St9 St10 St11 St15 St17 St19
f)
PO43- (µM)
0.0
0.1
0.2
0.3
0.4
0.5
0.6
St1 St4 St2 St3 St9 St10 St11 St15 St17 St19
g)
DOC (µM)
0
10
20
30
40
50
60
70
80
St1 St4 St2 St3 St9 St10 St11 St15 St17 St19
h)
aCDOM (m-1)
0.0
0.5
1.0
1.5
2.0
2.5
St1 St4 St2 St3 St9 St10 St11 St15 St17 St19

Figure 11

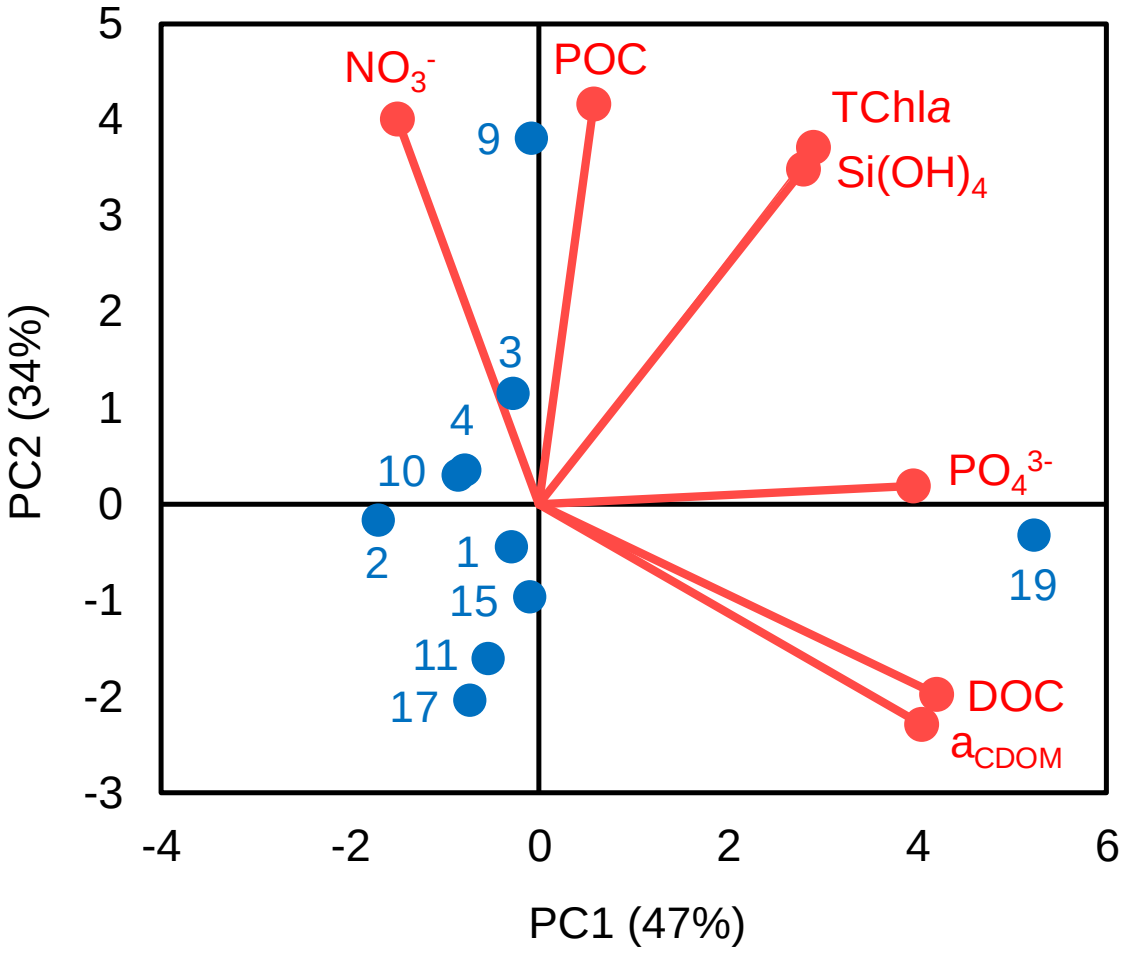
5
4
3
2
1
0
-1
-2
-3
PC2 (34%)
-4
-2
0
2
4
6
PC1 (47%)
NO3-
POC
TChla
Si(OH)4
PO43-
DOC
aCDOM
9
3
4
10
2
1
15
11
17
19

Figure 12

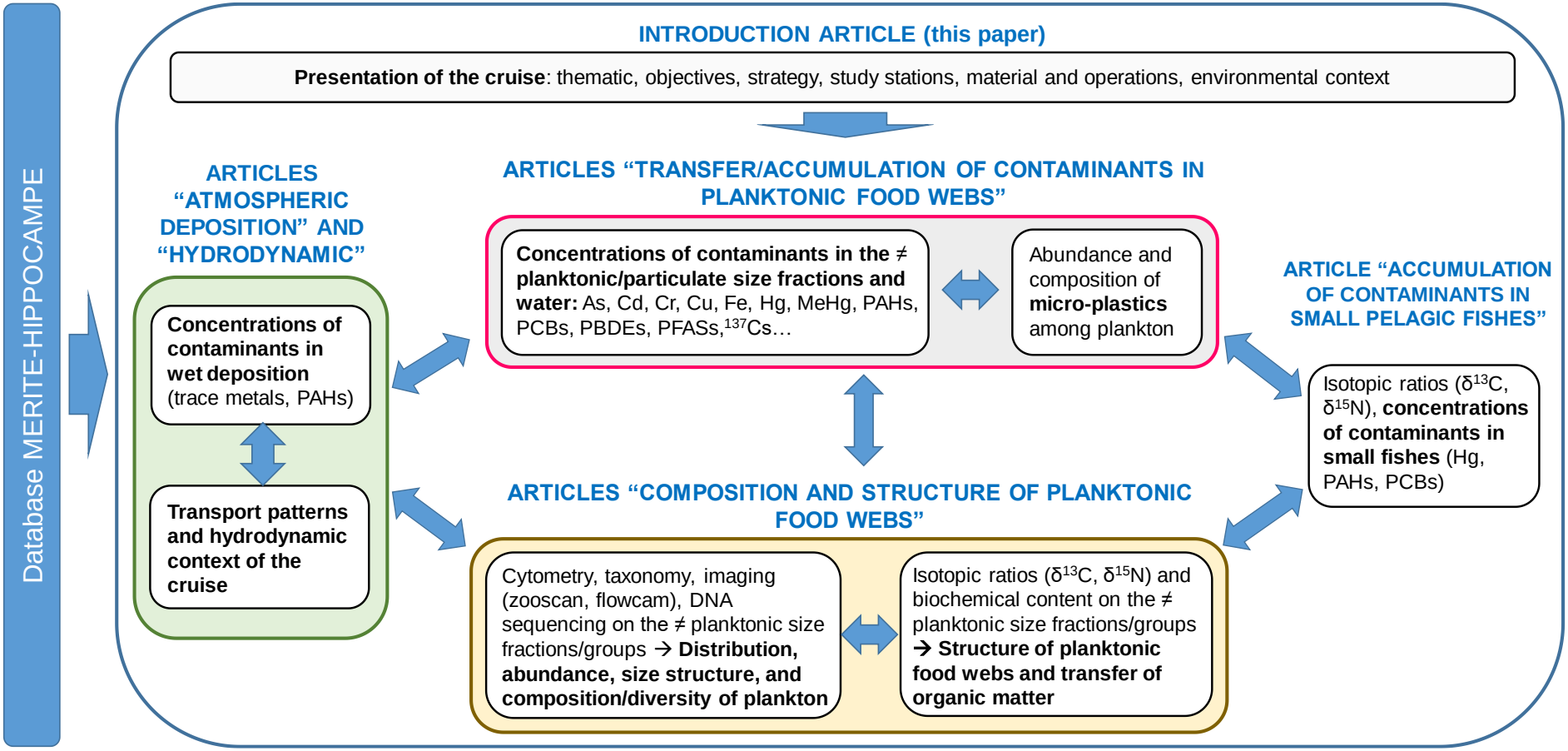
Database MERITE-HIPPOCAMPE
INTRODUCTION ARTICLE (this paper)
Presentation of the cruise: thematic, objectives, strategy, study stations, material and operations, environmental context
ARTICLES "ATMOSPHERIC DEPOSITION" AND "HYDRODYNAMIC"
Concentrations of contaminants in wet deposition (trace metals, PAHs)
Transport patterns and hydrodynamic context of the cruise
ARTICLES "TRANSFER/ACCUMULATION OF CONTAMINANTS IN PLANKTONIC FOOD WEBS"
Concentrations of contaminants in the ≠ planktonic/particulate size fractions and water: As, Cd, Cr, Cu, Fe, Hg, MeHg, PAHs, PCBs, PBDEs, PFASs, 137Cs…
Abundance and composition of micro-plastics among plankton
ARTICLES "COMPOSITION AND STRUCTURE OF PLANKTONIC FOOD WEBS"
Cytometry, taxonomy, imaging (zooscan, flowcam), DNA sequencing on the ≠ planktonic size fractions/groups → Distribution, abundance, size structure, and composition/diversity of plankton
Isotopic ratios (δ13C, δ15N) and biochemical content on the ≠ planktonic size fractions/groups → Structure of planktonic food webs and transfer of organic matter
ARTICLE "ACCUMULATION OF CONTAMINANTS IN SMALL PELAGIC FISHES"
Isotopic ratios (δ13C, δ15N), concentrations of contaminants in small fishes (Hg, PAHs, PCBs)

Figure 13